OPTICAL PROBING OF HEMODYNAMIC RESPONSES *IN VIVO* WITH CHANNELRHODOPSIN-2

by
Nadia Aleyna Scott

B.Sc., The University of Victoria, 2007

A THESIS SUBMITTED IN PARTIAL FULFILLMENT OF
THE REQUIREMENTS FOR THE DEGREE OF

MASTER OF SCIENCE
in
THE FACULTY OF GRADUATE STUDIES
(Neuroscience)

THE UNIVERSITY OF BRITISH COLUMBIA
(Vancouver)

July 2011

Abstract

Maintenance of neuronal function depends on the timely delivery of oxygen and glucose through changes in blood flow that are linked to the level of ongoing neuronal and glial activity, yet the mechanisms underlying this stimulus-dependent control of blood flow remain unclear. Here, using transgenic mice expressing channelrhodopsin-2 in a subset of layer 5b pyramidal neurons, we report that changes in intrinsic optical signals and blood flow can be evoked by activation of channelrhodopsin-2 neurons without direct involvement of other cell types. We have used a combination of imaging and pharmacology to examine the importance of glutamatergic synaptic signaling in neurovascular coupling. In contrast to sensory-evoked responses, we observed that glutamate-dependent neuronal signalling is not essential for the production of channelrhodopsin-evoked hemodynamic responses. Our results rather suggest that ChR2-activated neurons are coupled to the surrounding vasculature through a glutamate-dependent astrocytic pathway mediated by the Group I metabotropic glutamate receptor mGluR5.

Preface

Ethics approval for the research presented in this thesis was obtained from the University of British Columbia Animal Care Committee under protocols A09-0665 (Neuroplasticity) and A10-0140 (Neuroprotection).

Table of Contents

List of Tables

List of Figures

Acknowledgements

I thank all of my mentors at UBC who have further instilled in me a great love for science. In particular, I thank Dr. Tim Murphy for his quiet guidance and unerring passion for rigour.

I would also like to thank my fellow Neuroscience students and the Green College community at large for making graduate school way more fun than I ever thought it would be.

Special thanks to my family for always being there through thick and thin.

Chapter 1: Introduction

Aristotle, despite his questionable views on brain function, was perhaps closer to the mark when he claimed that, "the energy of the mind is the essence of life." Indeed, the brain is remarkably dependent on consistently high levels of energy; with even brief interruptions of this supply, neuronal death occurs and is succeeded by loss of life if energy levels remain insufficient. Why is the mammalian brain so subject to the consequences of energy failure, such as would occur during ischaemic stroke? Measures of brain energetics have confirmed that the brain consumes a disproportionate amount of energy in relation to its weight, accounting for 20% of an organism's glucose and oxygen utilisation during resting state, rather than the predicted 2%: the antithesis of the heat sink that Aristotle had envisioned. A corresponding disparity in the levels of cerebral blood flow – 10 % of cardiac output is destined for the brain – accompanies the high levels of cerebral energy utilisation. Together, these parallel mismatches are indicative of a functional relationship – neurovascular coupling – between cerebral activity and blood flow that has arisen under evolutionary pressure in order to ensure reliable energy levels for optimal neuronal function.

A brief history of neurovascular coupling research

The concept of functional hyperemia, whereby changes in cerebral blood flow are selectively matched to underlying changes in neuronal activity, is not a novel proposition. Rather, the earliest such mention of this phenomenon was proposed by the eminent Italian physiologist Angelo Mosso in 1881 who, in his recordings in human patients with skull defects, attributed the observed regional pulsations of the cortex to mental activity (Mosso, 1881, cited in Raichle, 1997). Further progress in the field, however, was hindered by experimental designs

that lacked adequate controls and accuracy. Thus, the research of Charles Roy and Charles Sherrington in 1890 represented a significant technological advancement, allowing them to extend Mosso's conclusions relating regional changes in blood flow to regional changes in brain activity. Using oncographic measurements from the cortical surface of anaesthetised dogs that allowed them to assess real-time changes in volume that were then correlated with simultaneous recordings of arterial and venous pressure, Roy and Sherrington first lent conclusive evidence to the theory that blood flow is locally regulated in the brain. Firmly contradicting the predominant view that blood flow could only be extrinsically regulated via changes in cardiac output and systemic blood pressure, they stated:

> Bearing in mind that strong evidence exists of localisation of function in the brain, we are of opinion that an automatic mechanism … is well fitted to provide for a local variation of the blood-supply in accordance with local variations of the functional activity. (p. 105)

Coupling these recordings with pharmacological manipulations of blood flow, Roy and Sherrington provided evidence that the intrinsic mechanism by which local vascular supply was varied was chemical in origin, leading them to conclude that, "the chemical products of cerebral metabolism contained in the lymph which bathes the walls of the arterioles of the brain can cause variations of the calibre of the cerebral vessels." This concept of neuronally-derived chemical derivatives would prove to be remarkably prescient in its anticipation of vasoactive agents.

Perhaps of equal importance, Roy and Sherrington recognised that capillaries, in addition to arterioles, contributed to functional hyperemia. Furthermore, they emphasised that redirecting blood flow to the brain was a protective measure that occurred "by sacrificing the

blood-supply of certain other parts of the body whose functional activity can be temporarily diminished or arrested without serious harm to the economy as a whole", thus highlighting the importance of providing energy to the brain over other organs such as the kidney.

Despite these early breakthroughs, however, demonstrated causality between neuronal activity and blood flow was not a foregone conclusion until the use of radioactive tracers – in particular 2-[^{14}C]-deoxyglucose – became prevalent (Sokoloff , 1981). With the development of positron emission tomography, the ability to record local metabolic and blood flow - 'hemodynamic' - changes in humans became possible, leading to the famous observation by Fox and Raichle that increases in cerebral blood flow far outstrip the concomitant changes in oxygen consumption (1986). Indeed, this substantive mismatch – the function of which remains unclear – now underlies the basis of the blood-oxygen-level dependent (BOLD) signal.

Based on their later identification of an activity-dependent increase in glucose consumption (35-50 %) that was disproportionate to the regional increase in utilised oxygen (5 %), Fox et al. (1988) challenged the assumption that the majority of energy used when neurons are activated comes from oxidative phosphorylation, rather advocating in favour of glycolysis as the predominant energy source during physiological neural activity. Although recent studies support a primary role for oxidative metabolism in the generation of ATP (Lin et al., 2010), other mechanisms, including lactate production through the astrocyte-to-neuron lactate shuttle, may also be involved (Pellerin & Magistretti, 1994; Pellerin et al., 1998; Wyss et al., 2011), although this is not without controversy (DiNuzzo et al., 2010). It is probable that energy sources vary in accordance with energy needs or are stimulus-dependent, thus accounting for much of the discrepancies between studies; it is even more likely that multiple energy production

mechanisms co-exist, each underlying different pathways in neurovascular coupling (Vanzetta & Grinvald, 2008; Jolivet et al., 2009).

Major hypotheses

While brain energy metabolism is unquestionably coupled to neuronal signalling, the energetic costs of neuronal activity remain elusive (Jolivet et al., 2009). Several conflicting calculations of the brain's energy budget have been proposed (Attwell & Laughlin, 2001; Nawroth et al., 2007; Jolivet et al., 2009), each with their methodological caveats. Despite their differences over relative proportions, it is generally accepted that the preponderance of cerebral energy consumption is devoted to the reversal of ion gradients following action potentials and synaptic potentials (Attwell & Laughlin, 2001).

According to the traditional metabolic hypothesis (Figure 1), neuronal activity produces rapid changes in glucose and oxygen concentrations that elicit an increase in the flow of oxygenated blood (Raichle & Mintun, 2006). In this negative feed-back system, a decrease in energy – signalled either by reductions in oxygen and glucose or an increase in carbon dioxide – triggers a compensatory increase in blood flow. Recent studies, however, have challenged this paradigm, demonstrating a more bilateral interaction between metabolism and neural activity whereby vascular changes – so-called anticipatory 'priming' hemodynamic events – precede neuronal events (Sirotin & Das, 2009). Still others have identified occurrences of disproportionate increases in blood flow in relation to the level of neuronal activity (Sirotin et al., 2009) and decreased blood flow in regions of high neuronal activity and glucose uptake (Devor et al., 2008). Perhaps most tellingly, increases in blood flow occur even during experimentally-induced high levels of oxygenation, undermining the very premise of the metabolic hypothesis

(Lindauer et al., 2010). Together, these observations signify the improbability of a negative feed-back mechanism in the control of cerebral blood flow.

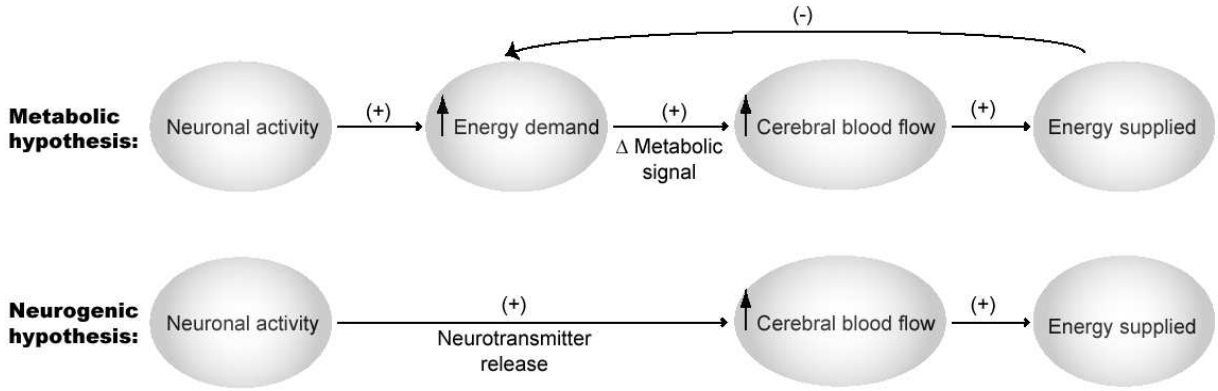

Figure 1. The major hypotheses of neurovascular coupling. Activity-induced changes in blood flow are hypothesised to occur either via a negative feed-back mechanism (above) or via a positive feed-forward mechanism (below). Adopted from Attwell et al., 2010.

Countering this, a model has been proposed that operates rather via feed-forward mechanisms (Figure 1). Alternatively referred to as the neurogenic hypothesis, this model permits the direct regulation of vascular energy supply by neural activity without the requirement for metabolic intermediaries (Hamel, 2006; Devor et al., 2008; Attwell et al., 2010). Here, either active neurons or astrocytes directly signal to blood vessels via the release of vasoactive agents, increasing the levels of blood flow. In contrast to the metabolic hypothesis, it is assumed that these neuronal and astrocytic pathways are mediated by neurotransmitter release, in particular glutamate (Attwell et al., 2010).

Glutamate-dependent neuronal control of vasculature

Glutamate is the primary excitatory neurotransmitter in the central nervous system, activating *N*-methyl-D-aspartate (NMDA), α-amino-3-hydroxy-5-methyl-4-isoxazolepropionic acid (AMPA) and kainate receptors. Of these, NMDA receptors have emerged as important players in neurovascular coupling. Although they display significant amino acid sequence similarity to that of AMPA/kainate receptors (Moriyoshi et al., 1991), they differ significantly from other ligand-gated ionotropic receptors in that extracellular Mg^{2+} confers a voltage-dependent block on the ion channel, uniquely allowing NDMA receptors to function as molecular coincidence detectors whereby both pre- and postsynaptic neurons must be excited for ion flow to occur. Especially contributing to their unique role in physiology is their high permeability to Ca^{2+} ions, initiating long-term potentiation and depression.

Upon synaptic release of glutamate from excitatory neurons, neuronal NMDA receptors become activated, leading to calcium entry and the downstream activation of neuronal nitric oxide synthase (nNOS). Several lines of evidence – from inhibition of nNOS to nNOS knockout mice to alternate NO donors – have implicated the subsequent production and release of nitric oxide (NO) in the dilation of blood vessels (reviewed in Attwell et al., 2010), both in the cortex and cerebellum (see Figure 2). In addition, it is has been suggested that the role of NO is more modulatory in nature, acting on astrocytic-dependent pathways (Lindauer et al., 1999).

Of significance to both the understanding of neurovascular coupling and the interpretation of functional imaging, it has also been demonstrated that activated inhibitory GABAergic interneurons are capable of mediating blood vessel constriction and dilation (Cauli et al., 2004; Kocharyan et al., 2008). While it remains unclear whether interneurons mediate their effects through direct signalling to the vasculature or via astrocytic intermediaries, it is certain that their involvement can no longer be ignored. Unquestionably, calculations of the

brain's energy budget would be vastly different if the participation of both excitatory and inhibitory interneurons were given equal consideration.

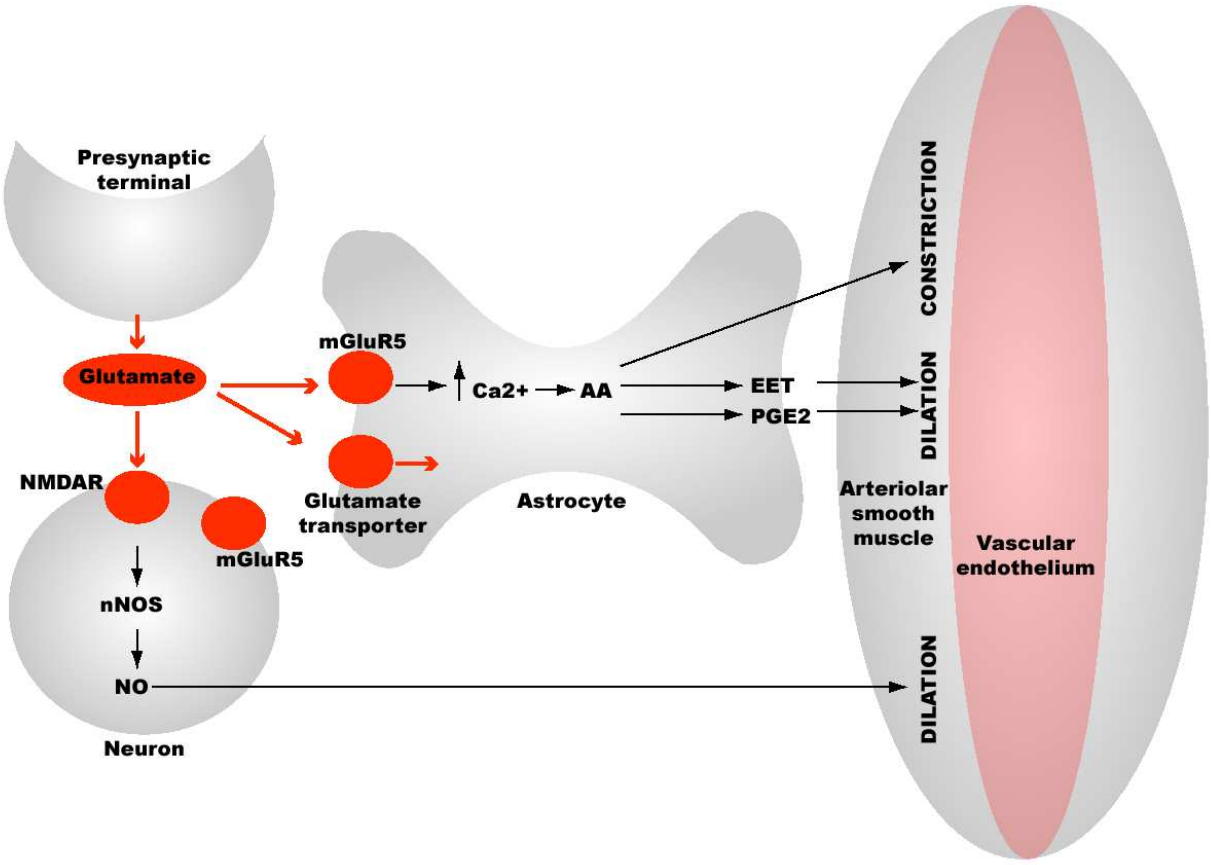

Figure 2. Glutamate-dependent pathways in neurovascular coupling. Presynaptic release of glutamate induces changes in arteriolar diameter via postsynaptic neuronal signalling or astrocytic release of vasoactive agents. Adopted from Koehler et al. (2009) and Attwell et al. (2010).

Glutamate-dependent astrocytic control of vasculature

Although the link between neural activity and cerebral blood flow appears from the outset to be a clearly delineated one, it is not immediately clear how flow may be matched to activity, both temporally and spatially. However, several lines of evidence have suggested that

astrocytes – as in the so-called 'tri-partite synapse' - may constitute the third player in neurovascular coupling.

Firstly, based on their morphology, grey matter (protoplasmic) astrocytes are ideally situated to translate regional synaptic activity to hyperemia as they extend processes that envelop both synapses and vasculature (Golgi, 1865, cited in Haydon & Carmignoto, 2006). Moreover, an individual astrocyte extends fine processes that are capable of sensing the activity of over one million synapses (Oberheim et al., 2006) and are in contact with at least one blood vessel; historically, the significance of this interaction in relation to neurovascular coupling was originally attributed to the ability of astrocytes to remove excess potassium ions – K^+ siphoning – from the synaptic cleft after high neuronal activity, leading to potassium efflux at the astrocytic endfeet and subsequent blood vessel dilation (Paulson & Newman, 1987). Furthermore, each astrocytic domain has minimal spatial overlap with neighbouring domains, thus resulting in the formation of glially-defined synaptic islands (Halassa et al., 2007). As a consequence of this, the organization of astrocytes has important implications for the efficiency and distribution of blood flow. Indeed, several authors have described evidence for laminar variations in astrocyte-vasculature interactions in the murine cortex, thus suggesting that spatial and temporal matching of blood flow to activity is determined by the cytoarchitectonics of specific cortical layers (Tsai et al., 2009; McCaslin et al., 2010). Using *in vivo* two-photon imaging, McCaslin et al. (2010) found that the laminar density of astrocytes showed distinct peaks at 40 to 60 and 440 to 500 μm below the cortical surface, mirroring the density of capillaries, which reached similar peaks at 30 to 40 μm and again at 500 μm; moreover, the average distance between astrocytes and capillaries decreased with increasing cortical depth. This, together with evidence from Tsai et al. (2009), who found that neuronal density peaks at 600 μm below the cortical surface, indicates a strong

correlation between the densities of neurons, astrocytes and blood vessels, suggesting that those columnar depths that carry the highest metabolic loads are best equipped to respond to these energy demands (Scott & Murphy, 2010).

Secondly, it has been observed that astrocytes respond to synaptic release of glutamate (Porter & McCarthy, 1996) with intracellular calcium oscillations (Pasti et al., 1997), indicating that astrocytes are reliable sensors of neuronal activity. Moreover, these oscillations are graded in frequency according to levels of neuronal activity (Pasti et al., 1997). When this is considered in light of the number of synaptic inputs received by a single astrocyte, it is apparent that astrocytes perform a similar role to the axon hillock in the summation of synaptic inputs.

Thirdly, these astrocytic elevations in intracellular calcium have been implicated in the release of vasoactive compounds - including ATP, eicosanoids (EETs), nitric oxide and cyclooxygenase - which have been demonstrated to depolarise smooth muscle cells, thus triggering the dilation of local blood vessels (Shi et al., 2008; Liu et al., 2011). Importantly, evidence suggests that *in vitro* activation of neurons triggers the formation of arachidonic acid in astrocytes, leading to the production and subsequent release of arachidonic acid derivatives, including prostaglandins and EETs (Alkayed et al., 1997), suggesting that functional hyperemia is mediated by the release of astrocytic derivatives *in vivo* (Liu et al., 2008; Koehler et al., 2009).

Linking these above observations, Zonta et al. (2003) were the first to examine whether neuronally-induced astrocytic calcium oscillations act as a bridge between neurons and blood vessels. To test this, the authors combined extracellular stimulation of neuronal afferents in cortical slice preparations while simultaneously imaging with two-photon microscopy to monitor changes in astrocytic calcium and dilation in arterioles. As hypothesised, electrical stimulation of neuronal afferents resulted in elevations in astrocytic calcium in both the somata

and endfeet. Remarkably, these astrocytic events correlated spatially with dilations in cortical arterioles, with such interactions only observed where endfeet were in close proximity with local vasculature. Further, the elevations in astrocytic calcium were also temporally correlated with dilation in arterioles, with the calcium peak at endfeet preceding the onset of arteriolar dilation by only one second (33 seconds and 34 seconds, respectively, from the onset of stimulation). Stimulus-induced calcium oscillations in astrocytes have been observed on a faster time scale *in vivo,* substantiating the role of astrocytes in the modulation of vascular tone (Winship et al., 2007).

Yet how is the relationship between neuronal activity and astrocytic calcium oscillations translatable into changes in microcirculation? Group I metabotropic glutamate receptors – including mGluR1 and mGluR5 – have been previously identified as key mediators in inducing astrocytic elevations in intracellular calcium upon synaptic release of glutamate (Porter & McCarthy, 1996; Pasti & Carmignoto, 1997); these subtypes couple to PLC, leading to increased inositol triphosphate and intracellular calcium (Vermeiren et al., 2005). Of these, mgluR5 expression is primarily astrocytic, making it an ideal target for pharmacological blockade; its expression on neurons is limited to the periphery of synapses or extrasynaptically (Biber et al., 1999; Vermeiren et al., 2005). If these calcium elevations in astrocytes are indeed essential in the control of microcirculation, the specific blockade of Group I metabotropic glutamate receptors should impair the ability of astrocytes to induce arteriolar dilations. In accordance with this, Zonta et al. (2003) observed reductions both in the elevation of astrocytic calcium and in arteriolar dilations upon neuronal afferent stimulation in the presence of mGluR1 and mGluR5 antagonists *in vitro*, while no changes to neuronal calcium elevations were apparent. These experiments were further corroborated by reductions in blood flow observed *in*

vivo by the same authors and by others (Sloan et al., 2005; Shi et al., 2008, Wang et al., 2006). Further pharmacology has identified the calcium-dependent activation of cyclooxygenase-1 and release of vasoactive prostaglandins as the primary downstream pathway of astrocytic mGluR5 activation (Zonta et al., 2003; Takano et al., 2006). Similar results were obtained in the murine olfactory bulb, suggesting a common glutamate-dependent astrocytic pathway (Petzold et al., 2008). However, glutamate uptake by sodium-dependent transporters has also been shown to be involved, suggesting that alternate glutamate-dependent pathways to mGluR5 play a substantial role in the elevation of astrocytic calcium levels (Gurden et al., 2006; Blanco et al., 2008).

Thus, conclusive evidence supports the theory that astrocytes act as bridges between the synaptic release of glutamate and changes in blood vessel diameter (see Figure 2). Recent research suggests that this dynamic control by astrocytes is modulated in accordance with oxygen levels, leading to either vasodilation or vasoconstriction (Gordon et al., 2008) in relation to a delimited set point (Blanco et al., 2008).

Optogenetics

Within the last five years, the neuroscience field has been quick to embrace the emerging technology of optogenetics, which provides the ability to control the activity of user-defined cells through heterologous expression of light-activated ion channels. Chief among these proteins is Channelrhodopsin-2, which has become a versatile player in studies ranging from respiration (Alilain et al., 2008) to motor mapping (Ayling et al., 2009). Isolated from the green alga *Chlamydomonas reinhardtii* where it is involved in phototaxis (Sineshchekov et al., 2002) and photophobic (Govorunova et al., 2004) responses, ChR2 is a 737-aa light-sensitive ion channel that is permeable to protons and univalent and bivalent cations (Nagel et al., 2003). Sequencing analysis has revealed that ChR2 shares several conserved amino acids with the

proton pump bacteriorhodopsin - those defining the retinal-binding site and the H+-transporting network - and also with the chloride pump halorhodopsin (Nagel et al., 2003).

Nagel et al. (2003) were the first to demonstrate that illumination of heterologously expressed ChR2 was sufficient to control intracellular *p*Ca or membrane potential, with maximum currents evoked at ~470 nm. Subsequent expression in genetically-defined subpopulations of neurons proved the efficacy of transducing photons into neuronal activity *in vitro* (Boyden et al., 2005; Li et al., 2005; Ishizuka et al., 2006), in slice preparations (Ishizuka et al., 2006) and *in vivo* (Li et al., 2005; Nagel et al., 2005), with action potentials reliably evoked at frequencies reaching 30 Hz. Importantly, photo-activation of the presynaptic neuron was sufficient to drive both excitatory and inhibitory postsynaptic currents, indicating that ChR2 stimulation of presynaptic neurons induces synaptic transmission (Li et al., 2005).

Hypotheses and experimental approach

From an experimental standpoint, it is difficult to distinguish neuronal from astrocytic activity. Disentangling the relative importance of each pathway becomes even more intricate when one considers that the release of synaptic glutamate initiates calcium elevations in both cell types and with similar rise times (Winship et al., 2007). Historically, glutamate-dependent neuronal pathways have been thought to be the primary mediators in neurovascular coupling, but as argued by Attwell et al. (2010), much of the pharmacological and electrophysiological support ascribed towards this theory applies equally to astrocytic pathways. Indeed, one of the key pieces of evidence (Logothetis et al., 2001) in favour of postsynaptic neuronal signalling – the correlation of local field potentials (reflecting input and intracortical processing) with changes in blood flow – could be similarly correlated with astrocyte activation through mGluR5. Moreover, the neuronal contribution is itself complex, as noted above,

comprising both excitatory neurons and inhibitory interneurons. Further complicating the issue, excitatory neurons are not themselves a uniform entity and their ability to control blood flow is determined by their local connections, thus resulting in regional differences in neurovascular coupling (Sloan et al., 2010) and energy usage (Vaishnavi et al., 2010) according to the stimulated pathway (Enager et al., 2009).

In brief, it remains unclear which cell types – excitatory neurons, inhibitory interneurons or glia – mediate neurovascular coupling, as traditional studies of neurovascular coupling have been restricted by the inability to selectively control neuronal activity. Circumscribing these limitations, optogenetics would provide a unique approach in probing the involvement of specific cell types in the control of blood flow. Thus, in the present study we have employed channelrhodopsin-2 (ChR2) transgenic mice that express a photoactivatable non-specific cationic channel in layer 5b pyramidal neurons (Arenkiel et al., 2007), allowing us to selectively activate regions of the somatosensory cortex (Ayling et al., 2009). Our overall hypothesis is that direct *in vivo* activation of excitatory neocortical neurons is sufficient to produce measurable hemodynamic responses, or changes in oxygenation and blood flow. Our specific aims are to examine the role of postsynaptic neuronal signalling and astrocytic pathways in the mediation of neurovascular coupling. Further, we aim to explore the temporal and spatial colocalisations of these hemodynamic responses with respect to functional imaging.

Chapter 2: Methods

Animals and surgery

All animal procedures were performed in accordance with the University of British Columbia Animal Care Committee protocols. Adult channelrhodopsin-2 transgenic mice (line 18, stock 007612, strain B6.Cg-Tg(Thy1-COP4/EYFP)18Gfng/J; The Jackson Laboratory, Bar Harbor, ME) were initially anaesthetized with isoflurane (4% in air for induction, 1.5% for surgery) and craniectomized over the right sensorimotor cortex as previously described (Zhang & Murphy, 2007). Temperature (37±0.5°C) was maintained throughout the experiment using a feedback-regulated heating pad monitored by a rectal thermometer. In experiments involving no cortical application of pharmacological agents, the exposed brain was covered with 1-1.5% agarose (Type 3-A Sigma; A9793) dissolved in a HEPES-buffered (pH 7.3) physiological salt solution (135 mM NaCl, 5.4 mM KCL, 1 mM $MgCl_2$, 1.8 mM $CaCl_2$, and 5 mM HEPES) and sealed with a glass coverslip. Following surgery, isoflurane was discontinued and anaesthesia was maintained with ketamine (20 mg/ml)/xylazine (1 mg/ml), administered as necessary to maintain a constant level of anaesthesia. Heart rate and blood oxygen saturation were continuously monitored (Starr Life Sciences pulse oximeter, Oakmont, PA).

Optical imaging and stimulation

For photostimulation of channelrhodopsin2-expressing neurons, we used a 473 nm photoactivation laser (CrystaLaser BCL-473-050, Reno, NV) as previously described (Ayling et al., 2009). For forepaw electrical stimulation, a train of pulses was delivered by a stimulus isolator (World Precision Instruments, Sarasota, FL) through two 30-gauge needles inserted subcutaneously into the left forepaw. Our stimulus protocol (1.5 mA, 3 Hz, 1-4s) was adopted from the literature (Devor et al., 2008).

To visualize the cortex and vasculature, the surface of the brain was illuminated with green LEDs, while red LEDs (centred at 635 nm) were used for intrinsic optical imaging (IOS), with the depth of focus set to approximately 250 μm to blur the contribution of surface blood vessels (Figure 3). Intrinsic optical imaging allows the measurement of oximetric signals through the back-reflection of light (Vanzetta et al., 2008); at the wavelength used in the present study, the measurements comprise both changes in the oxygenation state of hemoglobin and blood volume (Frostig et al., 1990). All images were captured with a CCD Dalsa 1M60 camera, with image acquisition performed using EPIX XCAP software (Buffalo Grove, IL; v2.2) with an E1DB frame grabber (EPIX). For IOS, each run consisted of twenty trials separated by a 45 s intertrial interval to allow responses to return to baseline. For each trial, 50 frames over 5 s were obtained at 10Hz. These 8-bit images were integrated in 16 bits over repeated trials, from which the percentage change in 635-nm reflectance was calculated at 32-bit resolution by dividing the difference between pre- and post-stimulation images (35-42 images) by pre-stimulation images (8-15 images) using a custom-written ImageJ (NIH, Bethesda, MD) plugin (Harrison et al., 2009). Due to the oversaturation caused by the 473 nm stimulation laser, these frames were blanked; thus, blanks in the displayed temporal profiles of IOS responses reflect stimulus artifacts. The terms 'changes in 635 nm reflectance' and IOS responses are used interchangeably throughout the text.

To assess blood flow, we used laser speckle contrast imaging, which capitalizes on the flow of blood cells that causes blurring of interference patterns created by coherent light illumination (Briers, 2001; Dunn et al., 2001). Illumination was provided by a 784 nm 32 mW StockerYale SNF-XXX_885S-35 laser (Stocker & Yale, Salem, NH) with an Edmund anamorphic beam expander T47274 (Edmund Optics, Barrington, NJ) held on a

micromanipulator at a 30° angle (Figure 1). A polarizing filter was used to modulate laser output. As with the IOS data, laser speckle images were saturated during periods of 473 nm laser stimulation and were blanked accordingly. However, in later experiments, a 715 nm lowpass filter was used to prevent light from the 473 nm laser from entering the camera. Data with and without the lowpass filter was included in the present study. For stimulation trials, each run consisted of twenty trials separated by a 45 s intertrial period, with 100 images collected over 10s (10 Hz) using 10 ms exposure. Spatial laser speckle contrast was calculated using ImageJ (NIH) as described previously (Sigler et al., 2008; Zhang and Murphy, 2007), although here we took the inverse square of the laser speckle contrast as an approximation of blood flow (Cheng and Duong, 2007). Thus, it is important to note that with this calculation, an increase in speckle contrast (whiter values) reflects increased blood flow. The terms blood flow and 'speckle contrast' are used interchangeably throughout the text.

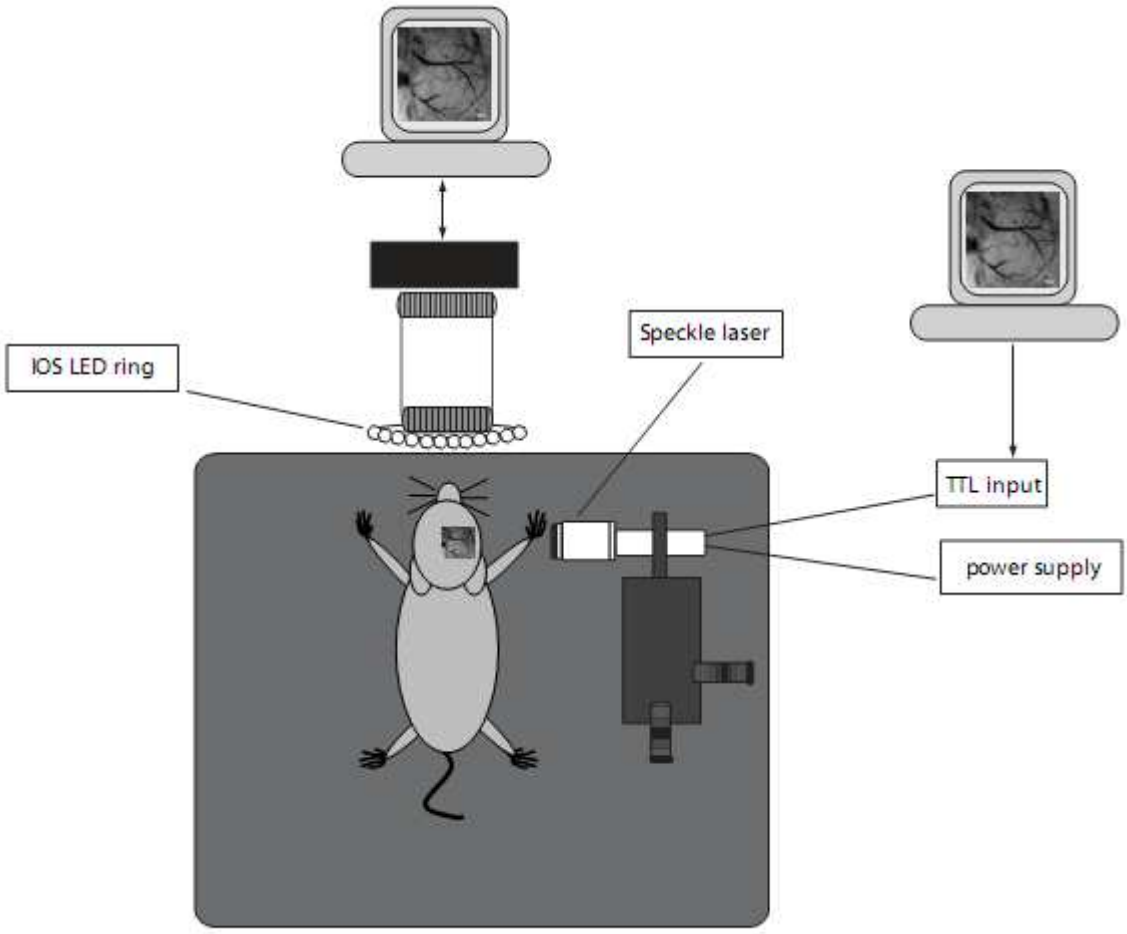

Figure 3. Schematic of imaging methods. Intrinsic optical signals (IOS) are revealed by reflected light from ring of red LEDs (centred at 635 nm). Laser speckle contrast imaging requires a diode laser (785 nm) positioned at an approximate angle of 30°. Both IOS and laser speckle imaging light sources are under TTL control.

Imaging analysis

For IOS and laser speckle data, temporal profiles were derived from ROIs (100 x 100 pixels) centered on the site of laser activation; profiles were smoothed (adjacent averaging) over 1 s prior to peak selection. Comparing responses by peak amplitude was compared to calculating the integral; both measurements produced similar results, but comparing peak

amplitudes was preferred due to its greater biological relevancy. Images for figures were Gaussian filtered (radius in pixels = 3 for IOS, 8 for speckle contrast) and speckle contrast images were averaged over 10 frames in ImageJ.

EEG Electrophysiological data were obtained in parallel with imaging sessions to compare stimulation-evoked EEG responses to hemodynamic changes. We placed a Teflon-coated silver wire on the surface of the cortex, with the reference electrode placed subcutaneously in the nose. The signal was amplified, filtered (0.2 kHz), and digitized (1000 Hz) using a differential AC amplifier (Model 1700, A-M Systems, Sequiem, WA), with data collected using Clampex 9.2 (Molecular Devices, Inc., Sunnyvale, CA). Traces were normalized and averaged using Clampfit 9.2 (Molecular Devices, Inc., Sunnyvale, CA). For spontaneous data, power spectrum analysis was performed using Clampfit 9.2 (Molecular Devices, Inc., Sunnyvale, CA). Frequency band analysis was performed to calculate the percentage of total power for the following defined frequency bands (Delta = 0.3-3 Hz; theta = 3-5 Hz,; alpha = 8-15 Hz; beta = 15-40 Hz; and gamma 40-80 Hz).

Pharmacology

To block intracortical synaptic transmission, we directly co-applied the ionotropic glutamate receptor antagonists CNQX (Sigma-Aldrich Co., Oakville, ON) and MK801 (Sigma-Aldrich Co., Oakville, ON) to the surface of the intact dura, at concentrations that we have previously demonstrated as sufficient to block sensory stimulation-evoked IOS maps (4.5 mM and 0.3 mM, respectively (Gurden et al., 2006), both in physiological saline solution). For these experiments, no agarose was placed on the cortex, and responses were found to be similar whether or not the dura was present. For our experimental procedures, animals were pre-imaged, followed by a minimum incubation time of 30 min with CNQX/MK801 and post-imaging.

Antagonists were reapplied to the cortex following each imaging run. To inhibit the Group I metabotropic receptor mGluR5, animals were pre-imaged, injected i.p. with MPEP (30 mg/kg; Tocris Bioscience, Ellisville, MO) and post-imaged after 20 minutes (for ChR2 stimulation experiments) and 40 minutes (for electrical forepaw stimulation experiments).

Statistics

All statistics were performed in GraphPad Prism (GraphPad Software, Inc.). All t-tests performed are two-tailed. Data are reported as mean ± SE; n=number of animals. Statistical significance on all figures uses the following convention: * $p>0.05$, ** $p>0.01$, *** $p>0.001$.

Chapter 3: Results

To assess whether activation of channelrhodopsin-2-expressing layer 5b neurons were sufficient to produce observable hemodynamic responses, we employed intrinsic optical signal (IOS) imaging (Grinvald et al., 1986; Frostig et al., 1990) and laser speckle imaging (Briers, 2001; Dunn et al., 2001) to observe signals that reflect changes in oxygenation and blood flow *in vivo*, respectively. Local targeting of blue collimated laser light (473 nm) through a coverslip-enclosed craniotomy allowed us to selectively stimulate channelrhodopsin-2-expressing neurons (Figure 4A) in the sensorimotor cortex with a high degree of spatial precision (Ayling et al., 2009). To compare these results with sensory stimulation, mice were given a brief shock to their forepaw.

Successful neuronal activation by ChR2 stimulation was confirmed by an evoked EEG response (Figure 4B), while parallel local changes in (apparent) oxygenation were assessed by measuring changes in the reflectance of 635 nm light, a wavelength that is sensitive to intrinsic optical signals (IOS) of oxyhemoglobin and deoxyhemoglobin (Figure 4C). We observed relative changes in IOS upon presentation of 1000 ms (n=23) trains of blue light stimulation (100 Hz stimulation) that paralleled responses evoked by forepaw stimulation (1000 ms, 3 Hz) in their time course (n=12) (Figure 4E). Both ChR2-evoked changes in EEG and IOS could also be evoked through a thinned skull preparation (n=2, data not shown) at amplitudes comparable to those evoked in craniectomized animals, thus obviating the requirement for invasive surgery

(Hira et al., 2009).

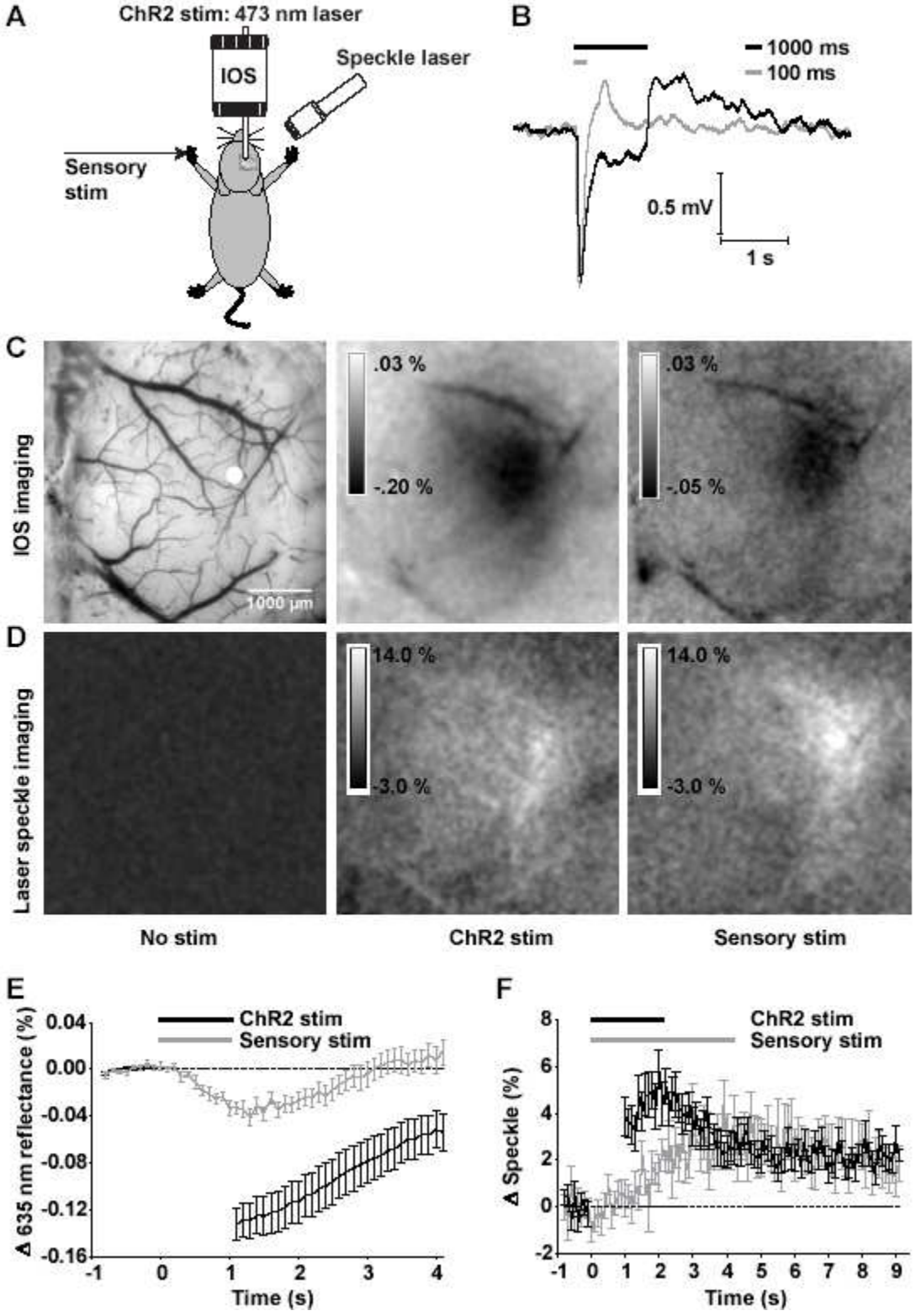

Figure 4. *In vivo* IOS and laser speckle imaging reveal that channelrhodopsin-evoked hemodynamic responses are of equal or greater magnitude to those evoked by forepaw stimulation. A, Schematic of experimental set-up. Responses to ChR2 stimulation (473 laser activation) and electrical forepaw stimulation were recorded via IOS imaging (635 nm) and laser speckle imaging (785 nm). B, Averaged EEG responses (20 trials) to 100 ms and 1000 ms of ChR2 stimulation in a representative animal. C, *left*: Green light image of the cortical surface. Peak IOS response (averaged over 1 s from peak) to 1 s of ChR2 stimulation (*middle*) and 1 s of forepaw stimulation (*right*). D, Maximum normalized laser speckle contrast response (averaged over 1 s at peak) to no stimulation (*left*), 1 s of ChR2 stimulation (*middle*) and 4 s of forepaw stimulation (*right*) in the same animal. C,D Data shown are averaged 20 trials from a representative animal. E, Temporal profiles of IOS responses evoked by 1 s of ChR2 stimulation compared to 1 s of forepaw stimulation (n=12). F, Temporal profiles of laser speckle responses evoked by ChR2 stimulus train durations of 1 s (n=13) compared to 4 s of forepaw stimulation (n=12). B,E-F Grey and black bars represent onset and duration of stimulation. Blanked data in temporal profiles reflect laser stimulus artifact. Error bars represent SEM.

To investigate whether functional hyperemia (elevated blood flow) were associated with these apparent changes in oxygenation (IOS signals), we used laser speckle contrast imaging at 785 nm to monitor changes in blood flow over large areas (Figure 4D). We observed changes in normalized speckle contrast upon presentation of 1000 ms (n=13) trains of

ChR2 stimulation, indicating that ChR2 stimulation could robustly evoke changes in blood flow that were of equal or greater magnitude to those evoked by forepaw stimulation (n=12) (Figure 4E). For both IOS and speckle contrast responses, temporal profiles were blanked during periods of laser stimulation.

ChR2 stimulation in channelrhodopsin-2-negative mice produced no observable change in EEG, IOS or speckle contrast, indicating that these effects are specific to mice expressing channelrhodopsin (Figure 5). For these control experiments, negative littermates were used (n=2).

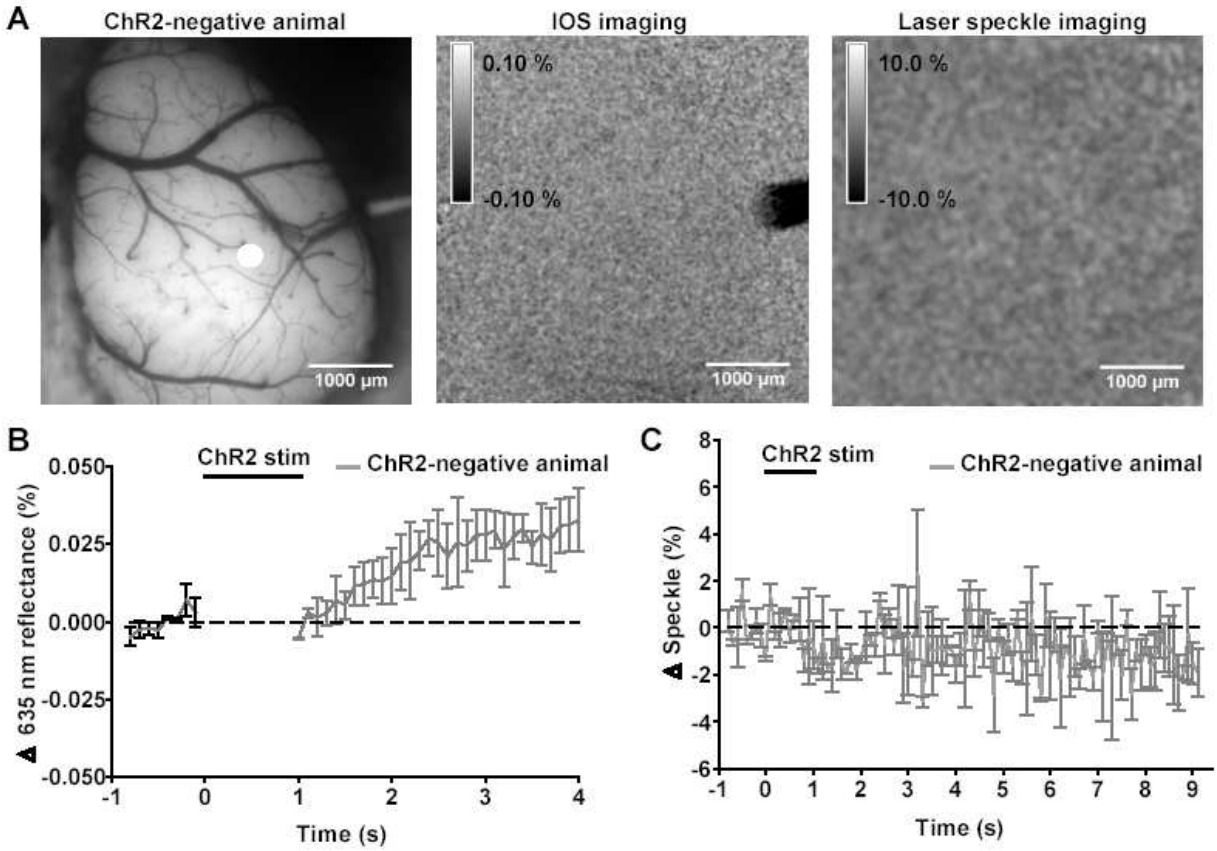

Figure 5. No channelrhodopsin-evoked hemodynamic responses are observed in non-channelrhodopsin-expressing animals. A, *left*: Green light image of the cortical surface, peak IOS response (averaged over 1 s from peak) (*middle*) and

peak normalized laser speckle contrast response (averaged over 1 s at peak) (*right*) to 1 s of ChR2 stimulation; data shown are averaged 20 trials from a representative animal. B, Temporal profiles of IOS responses evoked by ChR2 stimulation. C, Temporal profiles of laser speckle responses evoked by ChR2 stimulation. B,C Black bars represent onset and duration of stimulation. Blanked data in temporal profiles reflect laser stimulus artifact. Error bars represent SEM. N=2.

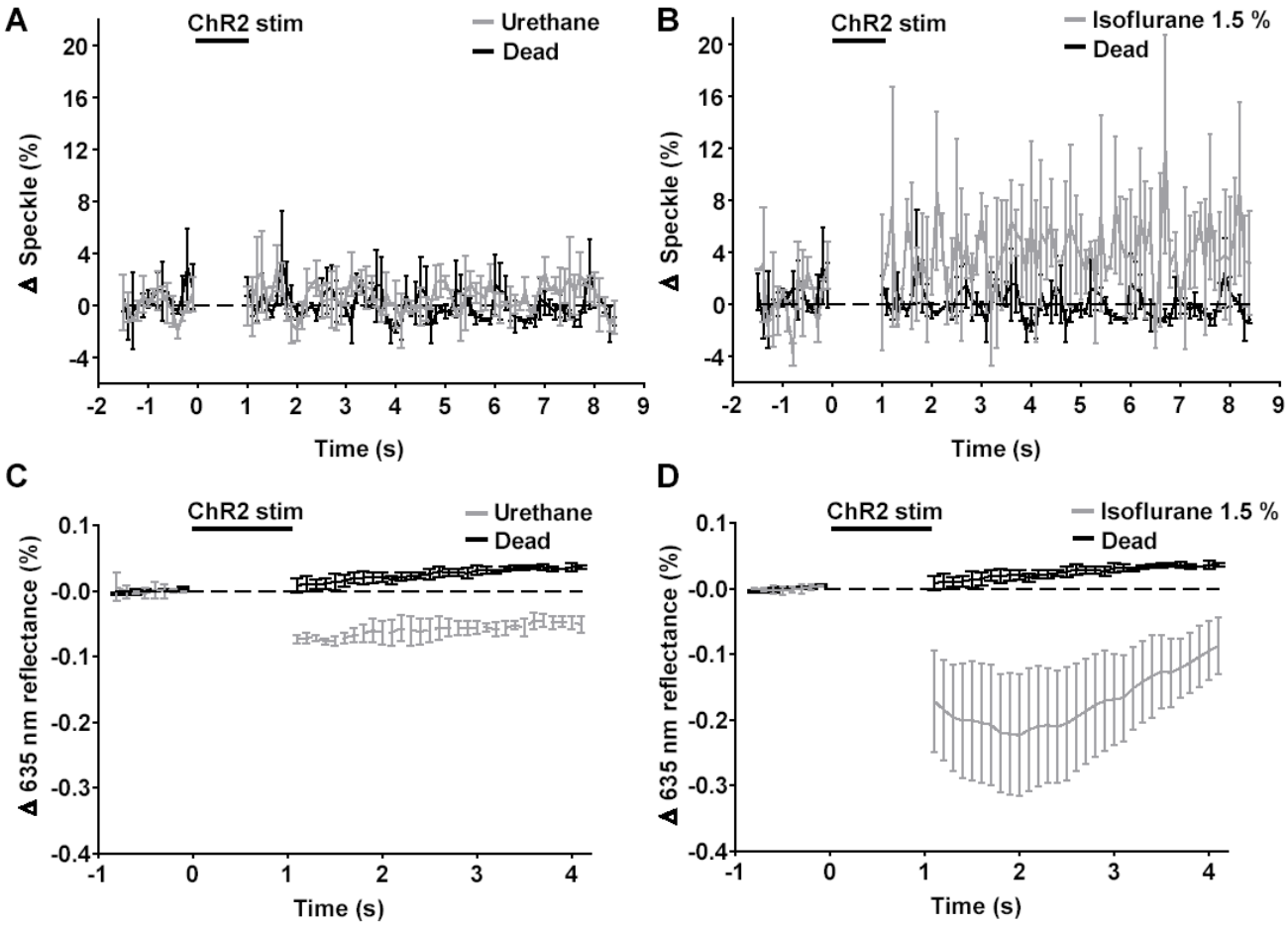

Figure 6. Effect of different anaesthesia on ChR2-evoked hemodynamic responses. Temporal profiles of laser speckle responses evoked by ChR2 stimulation under urethane (A; n=2) and isoflurane anaesthesia (B, n=2), compared to those evoked in dead animals (n=2). Temporal profiles of IOS responses evoked by ChR2 stimulation under urethane (C; n=2) and isoflurane anaesthesia (D, n=2), compared to those evoked in dead animals (n=2).

In a small number of animals, stimulation experiments were performed under different anaesthesias in order to determine whether the observed effects were specific to ketamine anaesthesia. Under either urethane or isoflurane anaesthesia, ChR2-evoked changes in speckle contrast were undifferentiable from responses evoked in dead animals (Fig 6A,B; n=2). However, IOS responses could be evoked from ChR2 stimulation under either urethane or isoflurane anaesthesia (Fig 6C,D; n=2). For the present study, ketamine anaesthesia was preferred over isoflurane as changes in blood flow could be more reliably observed.

In order to determine the effect of ChR2 stimulation on resting neural activity, we examined the power spectra of spontaneous EEG activity recorded (10 minutes) immediately prior to and following 20 trials of ChR2 stimulation (100 Hz, 1 s duration). No significant effect of ChR2 stimulation ($F(1,25) = 0.15$, $p = 0.7042$, $n = 6$) was observed in any frequency band (Fig 7B; Bonferroni post-test, all bands $p > 0.05$). To test for possible negative effects of ChR2 laser stimulation on the cortex, we focussed the laser on the forepaw sensory map and examined the amplitudes of sensory-evoked IOS maps before and after 20 trials of ChR2 stimulation. No difference in temporal profiles (Fig 7C; $F(1,200) = 2.37$, $p = 0.1253$) and peak amplitudes of evoked sensory maps before ($\Delta I/I$ -0.026 ± .004 %) and after ($\Delta I/I$ -0.031 ± 0.004 %) ChR2

stimulation were found (Fig 7D; n=5, p=0.3463, paired t-test), suggesting no profound effect of ChR2 stimulation on cortical function.

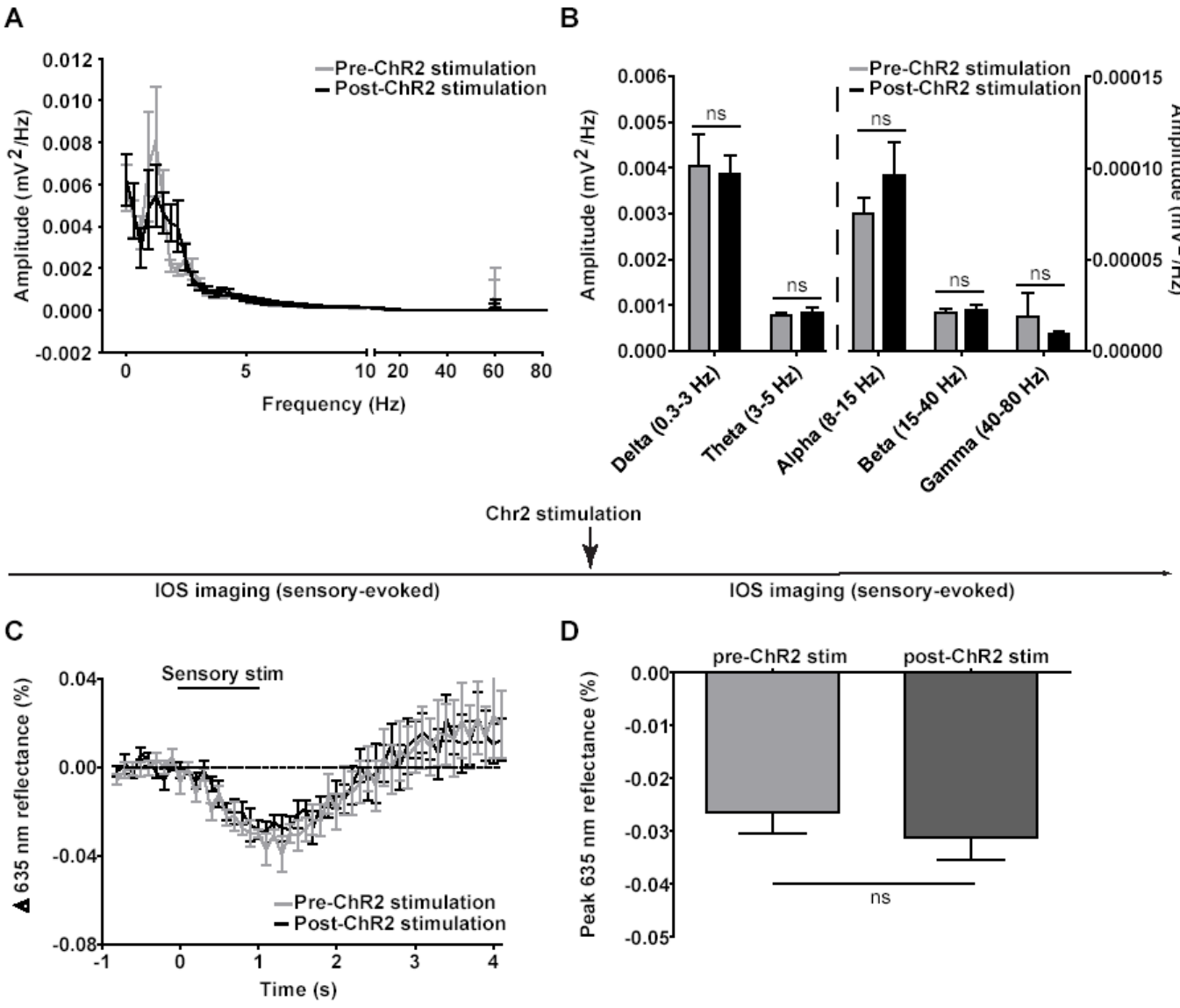

Figure 7. Effect of ChR2 stimulation on spontaneous EEG activity and sensory-evoked IOS responses. A, Power spectrum analysis of spontaneous EEG recordings before (gray) and after (black) 20 trials of ChR2 stimulation. B, Power spectra in (A) compared by frequency band. No significant effect of ChR2 stimulation was observed (Bonferroni post-test, all $p>0.05$, n=6). C, Temporal

profiles of sensory-evoked IOS responses evoked before (gray) and after (black) 20 trials of ChR2 stimulation. D, Peak responses of temporal profiles in (C) before and after ChR2 stimulation. No significant difference was observed (paired t-test, p=0.3463, n=5).

Likewise, ChR2 stimulation had no significant effect on either heart rate and O_2 saturation measurements (Bonferroni post-test, both $p > 0.05$) during 20 trials of ChR2 stimulation in comparison to measurements obtained prior to ChR2 stimulation (Table 1; repeated measures ANOVA, $F(1,6) = 0.01$, $p = 0.9384$), although there was a significant effect on variance for oxygen saturation.

Table 1. ChR2 stimulation does not have a significant effect on O_2 saturation or heart rate (repeated measures ANOVA, $F(1,6) = 0.01$, $p = 0.9384$).

	Baseline	ChR2 stimulation
0^2 saturation (%)		
Mean ± SEM	97.65 ± 0.94	98.61 ± 0.21
Range	(95.22 - 99.67)	(98.38 - 99.25)
Heart rate (bpm)		
Mean ± SEM	261.45 ± 20.40	258.39 ± 22.91
Range	(211.46 - 309.37)	(206.44 - 301.49)

To determine whether ChR2-evoked hemodynamic responses were graded according to stimulus duration, as has been observed for sensory-evoked hemodynamic responses (Nemoto et al., 2004), we examined the effect of increasing stimulus train duration on peak changes in IOS and speckle contrast (Fig 8).

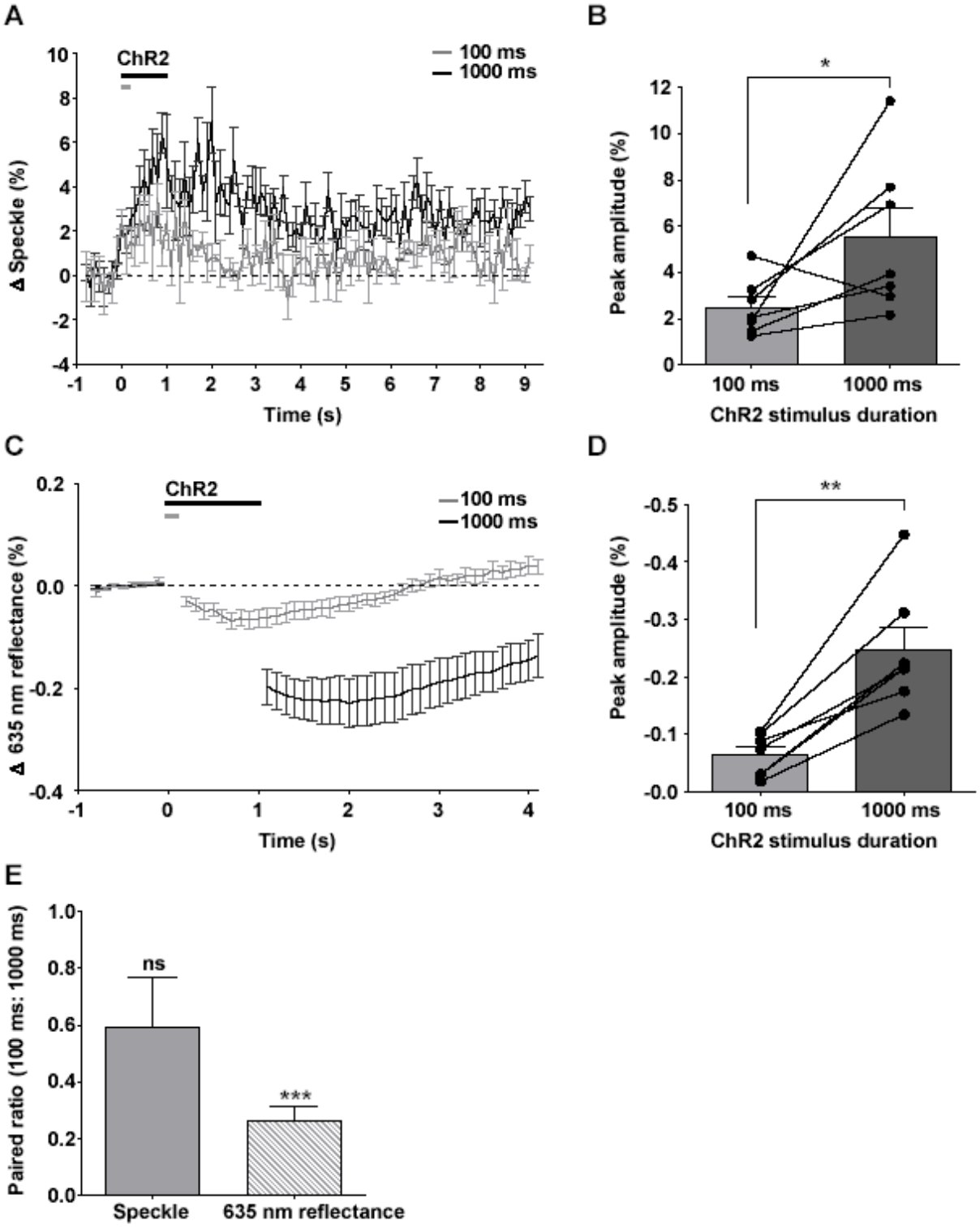
A
ChR2
100 ms
1000 ms
Δ Speckle (%)
Time (s)
B
*
Peak amplitude (%)
100 ms
1000 ms
ChR2 stimulus duration
C
ChR2
100 ms
1000 ms
Δ 635 nm reflectance (%)
Time (s)
D
**
Peak amplitude (%)
100 ms
1000 ms
ChR2 stimulus duration
E
Paired ratio (100 ms: 1000 ms)
ns
***
Speckle
635 nm reflectance

Figure 8. Effect of varying ChR2 stimulus train duration on evoked hemodynamic responses. A, Temporal profiles of laser speckle responses evoked by 100 ms (gray, n=7) and 1000 ms of ChR2 stimulation (black, n=7). B, Peak responses of temporal profiles in (A), compared within the same animals ($p = 0.0299$, ratio t-test of log-transformed values, n=7). C, Temporal profiles of IOS responses evoked by 100 ms (gray, n=7) and 1000 ms of ChR2 stimulation (black, n=7). D, Peak responses of temporal profiles in (C), compared within the same animals ($p = 0.0012$, paired t-test, n=7). E, Paired ratios of laser speckle responses (peak responses evoked by 100 ms: peak responses evoked by 1000 ms ChR2 stimulation) do not significantly differ from the hypothetical mean (one-way t-test; $p = 0.0594$), while those of IOS responses are significantly different from the mean (one-way t-test; $p < 0.0001$).

We found that maximal changes in speckle contrast were significantly greater (Fig 8A,B; $p = 0.0299$, ratio t-test of log-transformed values, n=7) when stimulated with 1000 ms trains (5.5 ± 1.3 s, n=7) compared to 100 ms trains (2.5 ± 0.5 s, n=7). Correspondingly, evoked changes in IOS were greater (Fig 8C,D; $p = 0.0012$, paired t-test, n=7) in response to 1000 ms stimulation ($\Delta I/I$ -0.25 ± 0.04 % change, n=7) than to 100 ms stimulation ($\Delta I/I$ 0.06 ± 0.01% change, n=7). Indeed, changes in IOS and speckle contrast could be reliably produced with as little as 10 ms of ChR2 stimulation. Paired ratios of laser speckle responses (peak responses evoked by 100 ms: peak responses evoked by 1000 ms ChR2 stimulation) did not significantly differ from the hypothetical mean (one-way t-test; $p = 0.0594$), while those of IOS responses

were significantly different from the mean (one-way t-test; $p < 0.0001$), suggesting greater sensitivity of IOS responses than changes in blood flow to stimulus duration.

Underscoring this, changes in IOS could be reliably evoked with a single 5 ms pulse (Fig 8A; n=5), while no changes in speckle contrast were discernable (Figure 9B; n=3).

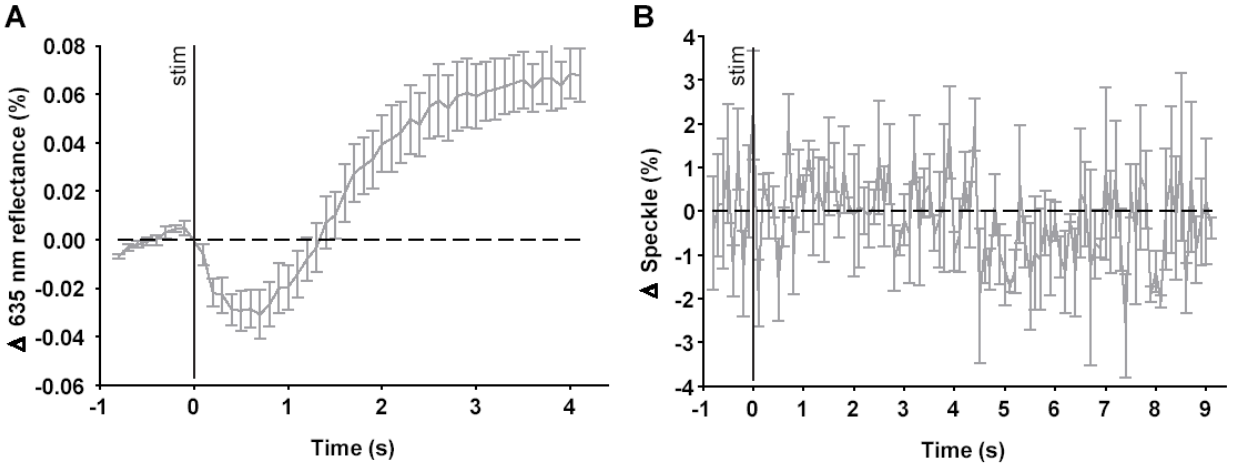

Figure 9. Greater sensitivity of IOS over speckle contrast to minimal (single 5 ms pulse) ChR2 stimulation. Temporal profiles of IOS responses evoked by a single 5 ms pulse (A; 20 trials; n=5). Temporal profiles of speckle contrast responses evoked by a single 5 ms pulse (A; 20 trials; n=3).

Convention holds that changes in oxygenation occur rapidly and are localized to the region of active neurons, while changes in blood flow occur more slowly and across greater area (Rossier, 2009). We compared the time to peak change in speckle contrast to that in IOS imaged within the same animals (Figure 10 A,B) to determine whether maximal changes in IOS peaked prior to maximal changes in blood flow. Normalising mean temporal profiles of IOS and speckle contrast responses to their relative maxima allowed us to visualize their times to peak (Fig 10A; n=6; one animal was excluded from this analysis because the peak occurred during the stimulus artifact). We found that maximal changes in IOS (635 nm reflectance) peaked at 1.2 ±

0.2 s after stimulus onset, while maximal changes in speckle contrast peaked at 1.1 ± 0.3 s (Fig 10B; paired t-test, p=0.7188, n=6). In comparison, maximal changes in IOS evoked by electrical forepaw stimulation peaked at 2.0 ± 0.4 s after stimulus onset (data not shown; n=4); indicating a slower time to peak in sensory-evoked responses.

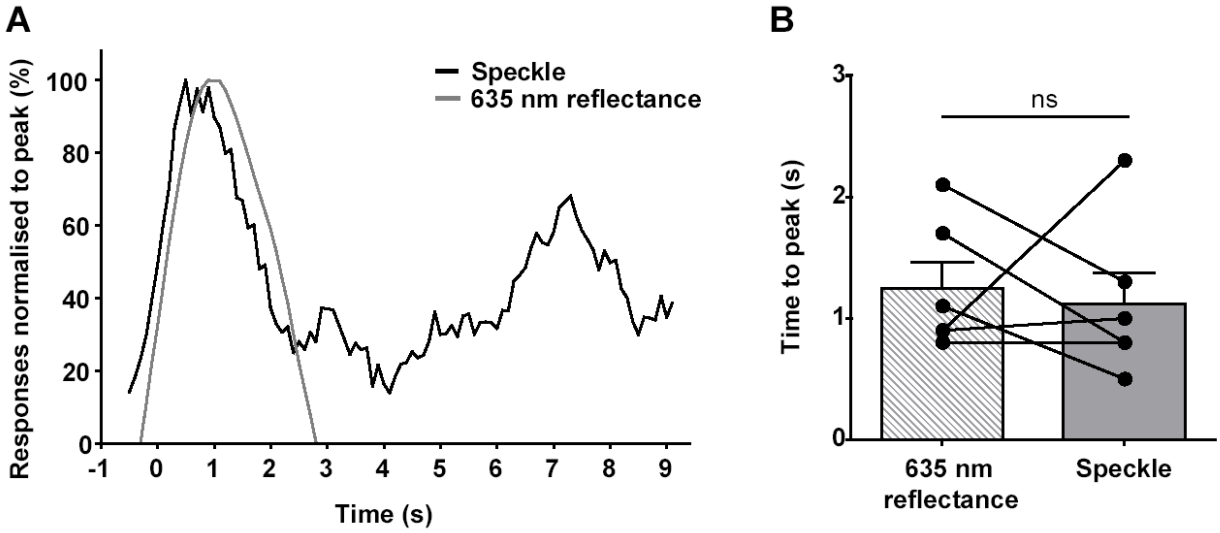

Figure 10. Comparing the time to peak of ChR2-evoked changes in IOS and laser speckle contrast. A, Averaged IOS responses (gray) and laser speckle contrast responses (black) to 100 ms of ChR2 stimulation were normalized to their maxima to highlight the differences in their times to peak, which are compared within animals in (B). No significant difference was observed (paired t-test, p=0.7188, n=6).

To examine whether ChR2-evoked IOS and blood flow responses differ in their spatial extent when measured in the same animals, we compared the peak amplitude of responses at increasing distances (500 μm increments) from the centre of activation (0 μm), which we

defined as the area of ChR2 laser stimulation (Fig 11 A,B). The peak amplitudes at each distance were normalized within each animal to peak amplitude at 0 μm prior to averaging over animals (n=6). For ChR2-evoked hemodynamic responses, our data indicate that IOS responses were localized to the site of laser activation, while blood flow responses were significantly more global (Figure 11A; $F(1,123)=43.71$, $p<0.0001$, 2-way ANOVA, n=6). There was a significant difference between the spatial extents of IOS and blood flow responses at distances greater than 1000 μm (all $p<0.001$, post-hoc Bonferroni). A similar effect was observed when we compared the spatial extent of forepaw stimulation-evoked IOS and blood flow responses measured in the same animals (Figure 11B; $F(1,64)=11.59$, $p=0.0012$, 2-way ANOVA, n=4), with significant differences in the spatial extent of IOS and blood flow responses observed at distances of 500 μm and 1000 μm (both $p < 0.05$).

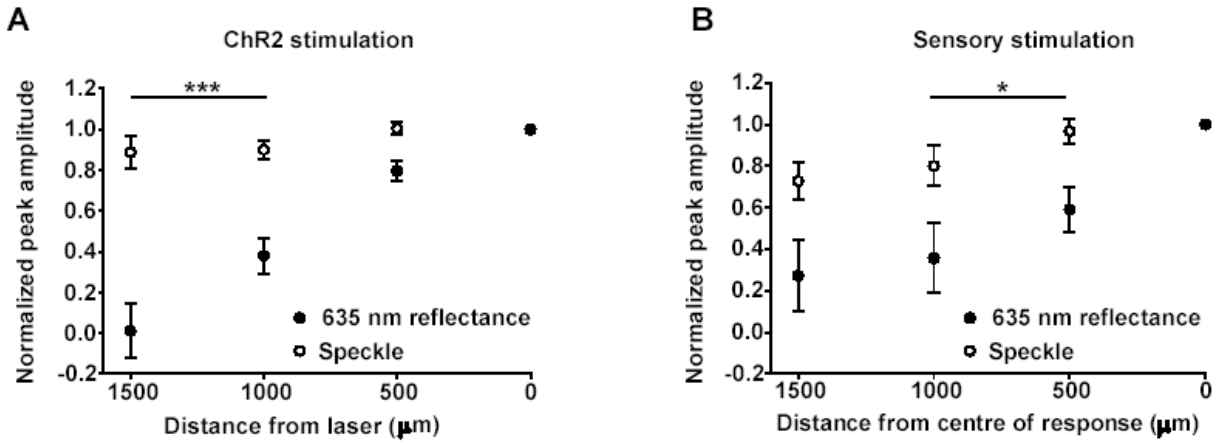

Figure 11. Comparing the spatial extent ChR2- and sensory-evoked changes in IOS and laser speckle contrast. The peak amplitudes of ChR2-evoked IOS and speckle contrast responses were compared as a function of distance from the centre of laser activation (Fig 8A). The spatial extents differed within animals at distances greater than 1000 μm (both $p < 0.001$, paired t-test, n=6). A similar

effect was observed in sensory-evoked IOS and speckle contrast responses at distances of 500 and 1000 μm (Fig 8B; both $p < 0.05$, paired t-test, n=4).

Postsynaptic activity has long been considered to be a primary determinant of neurovascular coupling (Atwell and Laughlin, 2001). To test whether ionotropic excitatory synaptic transmission were required for the production of hemodynamic responses, we first observed the effects of the AMPA receptor antagonist CNQX and the NMDA receptor antagonist MK801 on the changes in IOS evoked both by forepaw stimulation and direct activation of layer 5b neurons through ChR2 stimulation (Figure 12A). Following cortical incubation with CNQX/MK801, the IOS response evoked by 1 s of electrical forepaw stimulation in a representative animal was blocked, while the IOS response evoked by 1 s of ChR2 stimulation was preserved (Figure 12B). Peak changes in forepaw-evoked IOS responses obtained from temporal profiles in Figure 12C were significantly reduced following incubation with CNQX/MK801 (Figure 12E; paired t-test, p=0.0009, n=7), while no significant reduction was observed for ChR2-evoked IOS responses obtained from temporal profiles in Figure 12D (Figure 12E; paired t-test, p=0.9358, n=7). Interestingly, despite the lack of effect on the amplitude of ChR2-evoked IOS responses following CNQX/MK801 incubation, when we compared the slopes of linear regression lines fitted to the final second of the evoked IOS response, the slope of the post-antagonist response (0.05407 ± 0.004977, r^2=0.3544) differed significantly ($F(1,430)$=7.40507, p=0.006768) from that of the pre-antagonist response (0.03180 ± 0.006496, r^2=0.1003).

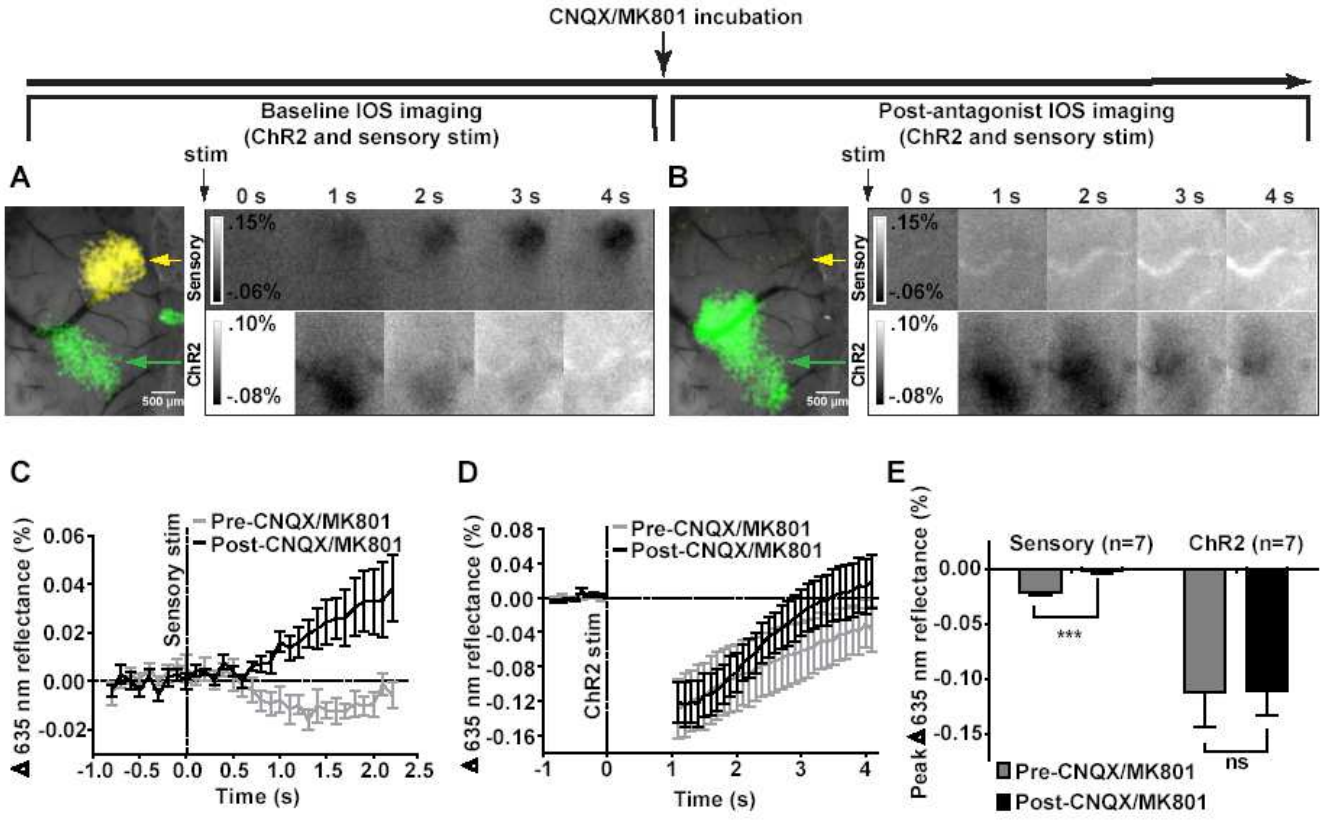

Figure 12. Blockade of intracortical ionotropic excitatory synaptic transmission by CNQX and MK801 inhibits the IOS response to forepaw stimulation, but not to ChR2 stimulation. A, *left*: Pre-antagonist IOS responses to forepaw stimulation (yellow, indicated by white arrow) and ChR2 stimulation (green, indicated by black arrow) thresholded to 50% of maximum and superimposed on an image of the cortical surface. *Right*: Temporal evolution of IOS responses to 1 s of forepaw stimulation (*upper*) and ChR2 stimulation (*lower*). B, *left*: Post-antagonist IOS response to forepaw stimulation is inhibited (white arrow indicates pre-antagonist map location), while the IOS response to

ChR2 stimulation is preserved (green, indicated by black arrow). *Right*: Temporal evolution of IOS responses to 1 s of forepaw stimulation (*upper*) and ChR2 stimulation (*lower*). A,B Shown are the averaged results of 20 trials from a representative animal. C, Temporal profiles of IOS responses to 1 s of forepaw stimulation before and after CNQX/ MK801 incubation (n=7). D, Temporal profiles of IOS responses to 1 s of ChR2 stimulation before and after CNQX/ MK801 incubation (n=7); blanked data indicate laser stimulus artifact. C,D Stimulus onset denoted by vertical dotted line. E, Peak changes in forepaw-evoked IOS responses were significantly reduced following antagonist incubation (paired t-test, p=.0009) while peak ChR2-evoked IOS responses were not significantly reduced (paired t-test, p=.9358). Error bars represent SEM.

To investigate whether functional hyperemia were comparably preserved when cortical tissue was stimulated by channelrhodopsin in the absence of intracortical ionotropic excitatory synaptic transmission, we examined changes in speckle contrast before and after incubation with CNQX/MK801 (Figure 13). We observed that channelrhodopsin-evoked laser speckle changes were intact following the blockade of ionotropic intracortical synaptic transmission in 5 animals (Fig 13A). No significant difference was observed in either the peak speckle contrast changes (Figure 13B; paired t-test, p=0.1370, n=5) or the time to peak of the response (not shown; paired t-test, p=0.2447, n=5) evoked before and after antagonist incubation. As expected, sensory-evoked changes in speckle contrast were significantly decreased upon incubation with CNQX/MK801 (Fig 13C; $F(1,700) = 155.67$; repeated measures ANOVA; $p < 0.0001$), with a significant reduction in peak speckle contrast (Fig 13C; paired t-

test, p = 0.0144, n = 8). These results indicate that activation of neurons through ChR2 leads to increases in blood flow that can occur independently of postsynaptic neuronal signalling.

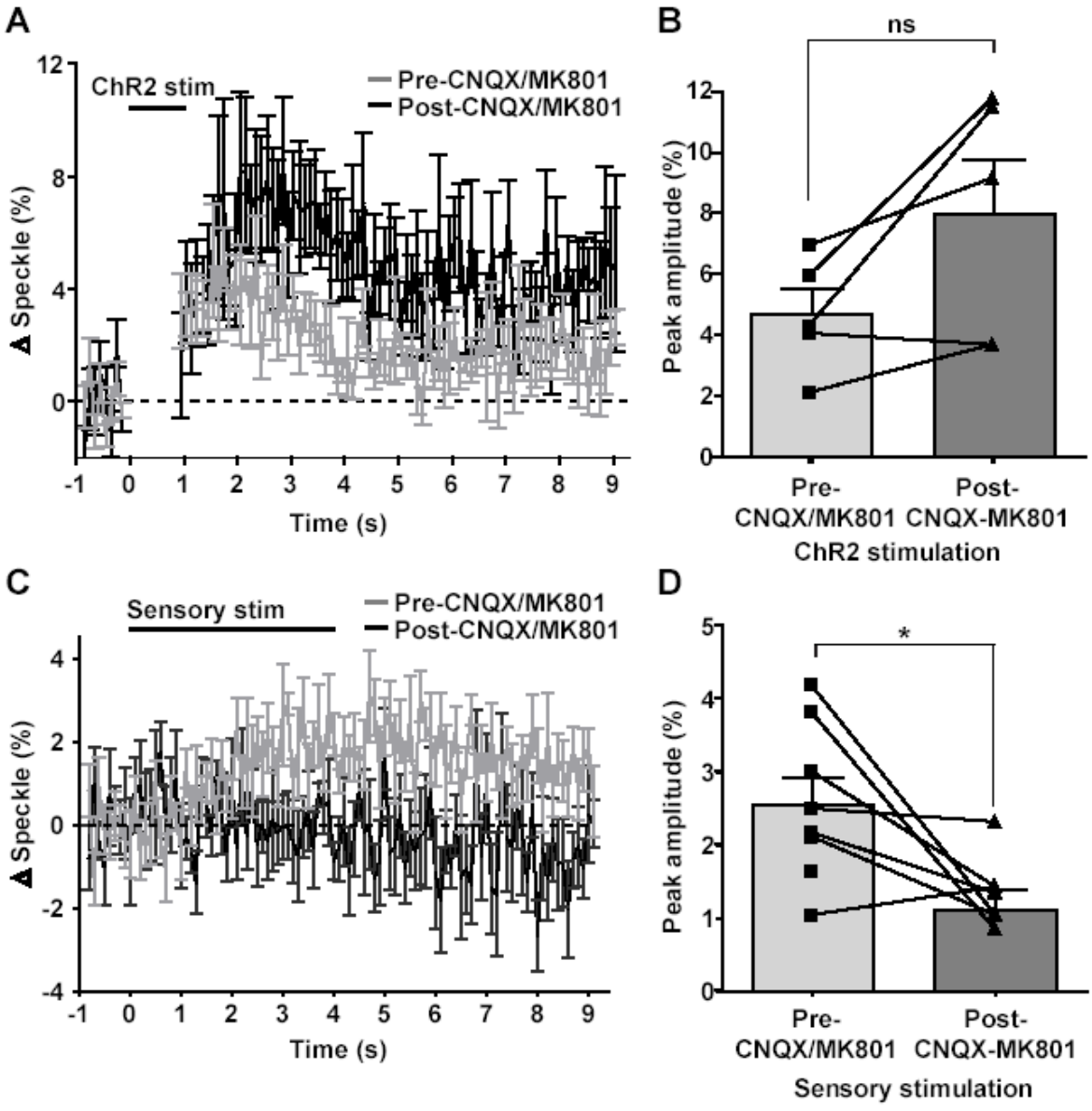

Figure 13. ChR2-evoked changes in blood flow are not inhibited by blockade of intracortical ionotropic excitatory synaptic transmission by

CNQX/MK801. A, Temporal profiles of laser speckle responses evoked by 1 s of ChR2 stimulation before and after antagonist incubation. B, Comparison of peak changes (averaged over 1 s) in laser speckle contrast responses in (A) before and after antagonist incubation. No significant difference was observed (paired t-test, p=0.1370, n=5). C, Temporal profiles of laser speckle responses evoked by sensory stimulation before and after antagonist incubation. D, Comparison of peak changes (averaged over 1 s) in laser speckle contrast responses in (C) before and after antagonist incubation. A significant difference was observed (paired t-test, p = 0.0144, n = 8). Error bars represent SEM.

It has been previously demonstrated that the astrocytic Group I metabotropic glutamate receptor mGluR5 couples presynaptic release of glutamate to changes in blood flow (Zonta et al., 2003). Our results with ChR2 stimulation suggest a similar astrocyte-dependent mechanism, with a significant reduction in ChR2-evoked speckle contrast following 20 minute incubation of the mGluR5 antagonist MPEP (Fig 14A; repeated measures ANOVA, $F(1,700)=59.62$, $p < 0.0001$, n=8). The peak Chr2-evoked speckle contrast was significantly reduced (Fig 14B; paired t-test, $p = 0.0251$, n = 8) from a pre-MPEP mean of 6.3 ± 1.4 % to a post-MPEP mean of 3.4 ± 0.9 %, resulting in a mean reduction of 33.70 ± 20.77 %. Half of the animals used for ChR2 stimulation were also examined for the effect of MPEP incubation on sensory-evoked speckle contrast, measured at 40 minutes post-MPEP incubation. As expected, MPEP incubation resulted in a significant reduction in sensory-evoked speckle contrast (Fig 14C; $F(1,300)=81.82$, $p<.0001$; two-way repeated measures ANOVA, n=4), with a significant (Fig 14D; $p = 0.0155$, t-test, n=4) reduction in peak speckle contrast observed, from a pre-drug

mean of 3.4 ± 0.9 to a post-drug mean of 2.3 ± 0.9, thus a mean reduction of 41.97 ± 7.40 %. While we examined the effects of MPEP incubation on ChR2-evoked IOS responses in 3 animals, no clear results were obtained (data not shown).

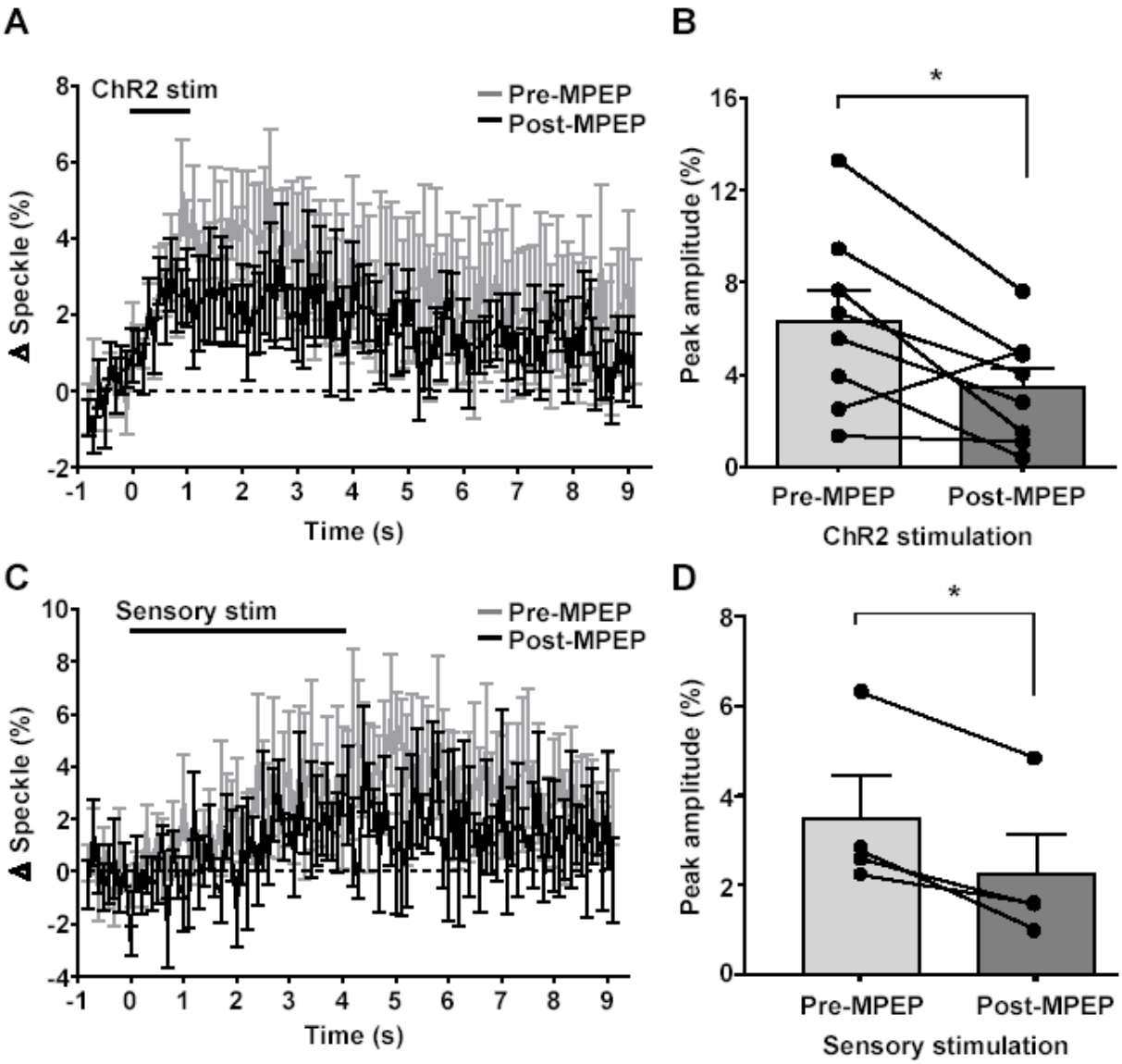

Figure 14. ChR2- and sensory-evoked changes in blood flow are inhibited by blockade of intracortical metabotropic excitatory synaptic transmission by MPEP. A, Temporal profiles of laser speckle responses evoked by 1 s of ChR2

stimulation before and after antagonist incubation. B, Comparison of peak changes (averaged over 1 s) in laser speckle contrast responses in (A) before and after antagonist incubation. A significant difference was observed (paired t-test, p = 0.0251, n = 8). C, Temporal profiles of laser speckle responses evoked by sensory stimulation before and after antagonist incubation. D, Comparison of peak changes (averaged over 1 s) in laser speckle contrast responses in (C) before and after antagonist incubation. A significant difference was observed (p = 0.0155, t-test, n=4). Error bars represent SEM.

To see the effects of MPEP on resting EEG, we examined 10 minutes of spontaneous EEG collected before and after MPEP injection (up to 20 minutes post-injection). In 4 animals, we compared the power spectra of spontaneous EEG before and after and observed a significant effect of MPEP on the power spectra (Fig 15A; repeated measures ANOVA; $F(1,795)=11.39$; $p=0.0008$, n=4). When power spectrum amplitudes were compared by frequency bands (Fig 15B) before and after MPEP incubation, a significant effect of MPEP overall was observed (repeated measures ANOVA, $F(1,15)=6.13$, $p = 0.0257$, n = 4) but no significant difference before-after was observed for the described frequency bands (Bonferroni post-test, all $p>0.05$, n=4).

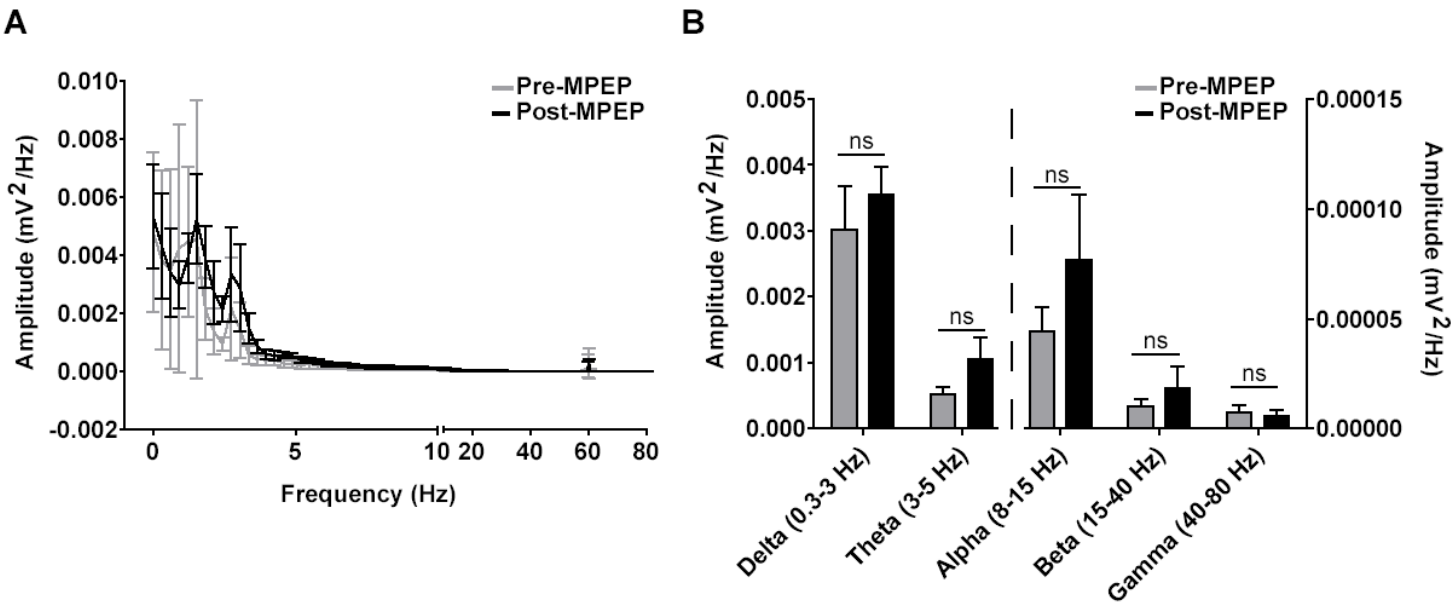

Figure 15. Effect of MPEP on spontaneous EEG activity. A, Power spectrum analysis of spontaneous EEG recordings before (gray) and after (black) MPEP injection. B, Power spectra in (A) compared by frequency band (Bonferroni post-test, all $p>0.05$, n=4).

In order to determine whether the observed reductions in blood flow responses upon MPEP incubation could be attributable to changes in underlying physiology, we compared heart rate and O_2 saturation recordings prior to MPEP incubation and at 0 minutes and 10 minutes post-MPEP incubation. No significant effect of drug incubation was observed (Table 2; repeated measures ANOVA, $p = 0.2308$, $F(2,8) = 1.77$, n=3), nor when all post-drug time points were compared to pre-drug averages (all $p < 0.05$ for O_2 saturation and heart rate, n=3).

Table 2. MPEP does not have a significant effect on O_2 saturation or heart rate (repeated measures ANOVA, p = 0.2308, F(2,8) = 1.77, n=3).

	Pre-MPEP	0 min post-MPEP injection	10 min post-MPEP injection
0^2 saturation (%)			
Mean ± SEM	99.38 ± 0.11	99.03 ± 0.22	98.92 ± 0.31
Range	(99.25 - 99.60)	(98.61 - 99.34)	(98.30 - 99.31)
Heart rate (bpm)			
Mean ± SEM	242.02 ± 37.72	236.58 ± 10.36	272.56 ± 22.44
Range	(188.25 - 314.73)	(217.35 - 252.89)	(244.20 - 316.86)

Chapter 4: Discussion

We have demonstrated that stimulation of channelrhodopsin-2-expressing pyramidal neurons is sufficient to evoke changes in oxygenation and blood flow, providing conclusive evidence that excitatory neurons are themselves able to initiate functional hyperemia when selectively activated, facilitated in part by the secondary involvement of other cell types. Attendant to this, the work presented here has validated the technique of optogenetics as a viable tool in the *in vivo* study of neurovascular coupling. Further, we have demonstrated that ChR2-evoked hemodynamic responses occur in the absence of ionotropic glutamatergic synaptic transmission, suggesting an independence of postsynaptic neuronal signalling. Together with a demonstrated dependency of these responses on mGluR5 activation, our results are thus consistent with a glutamate-dependent astrocytic neurovascular pathway, with minimal contribution from glutamate-dependent neuronal signalling.

Characteristics of Channelrhodopsin-evoked hemodynamic responses

We observed ChR2-evoked changes in IOS and blood flow that were comparable - both temporally and spatially - to those evoked by sensory (forepaw) stimulation, suggesting that the production of hemodynamic responses is determined by physiological constraints that are independent of stimulus modality. Moreover, we found that responses evoked by ChR2 were graded according to stimulus duration, indicating that the responses are not all-or-none, but rather sensitive to the duration of the stimulus train. It remains to be determined whether this phenomenon is due to the recruitment of more neurons, or to a greater release of neurotransmitter upon increased stimulus duration. However, our preliminary analysis suggests that neither IOS responses nor blood flow responses were increased in maximum areal extent upon increased stimulus duration, supporting the idea that surrounding neurons are not recruited with increased

stimulus duration. Interestingly, our data indicate that ChR2-evoked IOS responses are more sensitive to increases in stimulus duration than are ChR2-evoked blood flow responses, suggesting that changes in blood flow responses are less proportional in magnitude than changes in oxygenation to neuronal activity. Underscoring this, reliable changes in IOS can be evoked by ChR2 stimulus protocols that are unable to induce comparable changes in blood flow, even within the same animals. This phenomenon may relate to the theory that evoked changes in blood flow act as a 'safety factor'; according to this, changes in oxygenation are only observed when energy demands exceed that for which changes in blood flow can ably compensate (Sirotin et al., 2009). Thus, small changes in blood flow – such as may be masked by the noise inherent to laser speckle contrast imaging – may be accompanied by more obvious changes in oxygenation, highlighting a temporary mismatch between energy demands and energy supply. Despite cursory resemblance to the metabolic hypothesis, the concept of a safety factor is consistent with activity-driven feed-forward changes in blood flow.

Postsynaptic-independent mechanisms of neurovascular coupling

It has been well demonstrated that changes in oxygenation (Caesar et al., 2008; Lecoq et al., 2009) and cerebral blood flow (Norup Nielsen & Lauritzen, 2001; Chaigneau et al., 2007) are strongly coupled to local postsynaptic activity. As noted by Attwell et al. (2010), however, these correlations do not preclude a similarly significant astrocytic involvement. Further, previous studies have been constrained in that they were unable to directly activate specific neurons during blockade of synaptic transmission, a limitation that we have avoided through optogenetic stimulation. In the present study, we have observed that ChR2 stimulation of somatosensory neurons evoked changes in oxygenation and blood flow despite the concurrent

antagonism of postsynaptic ionotropic glutamate receptors, while sensory-evoked hemodynamic responses were greatly reduced, as others have consistently observed.

How might such a discrepancy between ChR2 stimulation and sensory stimulation arise? Comparable findings to those in the present study have been observed in the olfactory bulb, where sensory-evoked changes in IOS (Gurden et al., 2006) and blood flow (Petzold et al., 2008) were similarly elicited in the absence of ionotropic postsynaptic activity. This suggests that different brain regions have different requirements for glutamate-dependent neuronal signalling in accordance with their local anatomical connections. Such evidence for regional differences in neurovascular coupling has been noted by Sloan et al. (2010). However, our results suggest differences within the somatosensory cortex itself and are thus indicative of stimulus- and pathway-dependent variations in neurovascular coupling, lending support to the research of Enager et al. (2009).

It is of interest that our observed ChR2-evoked changes in blood flow were increased in magnitude upon blockade of postsynaptic ionotropic glutamate receptors. While the dichotomous effects of AMPA/NMDA receptor blockade on ChR2-evoked IOS (no change in magnitude, but steeper return to baseline) and speckle contrast (slight increase in magnitude) remain to be explored, such an observation is suggestive of interneuron-mediated inhibition through tonic activation of presynaptic GABA-B receptors, as consistently observed in the olfactory bulb (Pirez & Wachowiak, 2008; Petzold et al., 2008). Thus, the increased blood flow we observed could point to enhanced activation of astrocytic mGluR5 receptors through elevated presynaptic release of glutamate (Attwell et al., 2010). As another possibility, blockade of AMPA receptors may have induced a rapid increase in presynaptic function, resulting in elevated

presynaptic release of glutamate, as has been recently observed in this hippocampus (Jakawich et al., 2010).

Astrocytic-dependent mechanisms of neurovascular coupling

Mechanistically, the results of the present study suggest that ChR2-evoked presynaptic activity is coupled to functional hyperemia via astrocytic pathways (Figure 2) that operate independently of postsynaptic ionotropic glutamate receptors (Zonta et al., 2003). Indeed, studies of the olfactory bulb have demonstrated a role for presynaptic release of glutamate in triggering hemodynamic responses via astrocytic glutamate uptake transporters (Gurden et al., 2006) and metabotropic glutamate receptors, in particular mGluR5 (Petzold et al., 2008). In support of this, our results have suggested a role for mGluR5 in coupling ChR2-evoked presynaptic release of glutamate to elevations in blood flow. Although we observed mGluR-dependencies for both ChR2 and sensory stimulation, greater reductions were obtained for the latter (> 40 % versus 33 %, experiments performed in the same animals). Thus, it appears that while both stimulation pathways have an mGluR-dependent component, the effect of mGluR5 blockade is more acute for sensory-evoked activity. Our results substantiate the findings of Sloan et al. (2010) who similarly found disparities in blood flow reduction across the murine cortex upon mGluR5 blockade, which they attributed to local variations in excitatory versus inhibitory signalling.

Alternative mechanisms

Significantly, our blockade of NDMR/AMPAR had no effect on ChR2-evoked functional hyperemia, while mGluR5 blockade only attributed for ~ 33 % of the evoked response. Which pathways account for the remainder of the response? As observed by Gurden et al. (2006), Petzold et al. (2008) and Blanco et al. (2008), activation of mGluR5 is not the sole

glutamate-dependent astrocytic pathway. Rather, the above evidence is indicative of the involvement of alternative mechanisms, in particular glutamate uptake by the astrocytic sodium-dependent glutamate transporter (shown in Figure 2). In line with this, our preliminary experiments suggest that this transporter has a biphasic effect on the production of hemodynamic responses: at low concentrations of transporter antagonist, ChR2-evoked IOS responses are increased, while high concentrations lead to significant reductions in evoked IOS responses. Indeed, such results would appear to further substantiate the role of mGluR5, as glutamate spillover from mild transporter blockade would be expected to result in increased glutamate activation of mGluR5.

Alternatively, it is possible that vasoactive molecules (Hamel, 2006), released as a consequence of ChR2-initiated action potentials, act upon nearby capillaries or arterioles to produce changes in dilation and concomitant changes in blood flow, thus coupling spiking in activated layer 5b neurons to the surrounding vasculature. However, it is difficult to dissociate spiking from synaptic activity, as blocking action potential firing has a concomitant effect on synaptic transmission.

Summary

In conclusion, the results of the present study are as follows:

- Direct activation of excitatory cortical neurons in the rodent somatosensory cortex drives functional hyperemia, supporting the neurogenic hypothesis.
- Glutamate-mediated neuronal signalling is not the primary mediator of neurovascular coupling under ChR2 stimulation. However, we acknowledge that our findings do not preclude alternate mechanisms involving synaptic activation of intermediary neuronal populations.

- Synaptic release of glutamate does play a significant role in ChR2-evoked neurovascular coupling, albeit via glutamate-dependent astrocytic pathways through activation of the metabotropic glutamate receptor mGluR5

Future directions

Future experiments should address the following:

- Deconstruct neuronal activity to elucidate which component – spiking or neurotransmitter release – is most closely tied to the control of cerebral blood flow.
- Examine the role of neuronally-released vasoactive molecules such as NOS or cyclooxygenase.
- Determine whether these changes in blood flow are preceded by changes in astrocytic calcium.
- Examine whether ChR2-evoked changes in blood flow display laminar variations.
- Determine the secondary involvement of interneurons through immediate early gene expression following ChR2 stimulation.
- Address the specific role of astrocytes and interneurons through cell type-specific expression of ChR2 or another light-activated molecule.

Bibliography

Alilain WJ, Li X, Horn KP, Dhingra R, Dick TE, Herlitze S, Silver J (2008) Light-induced rescue of breathing after spinal cord injury. J Neurosci 28:11862-70.

Alkayed NJ, Narayanan J, Gebremedhin D, Medhora M, Roman RJ, Harder DR (1996) Molecular characterization of an arachidonic acid epoxygenase in rat brain astrocytes. Stroke 27:971-9.

Arenkiel BR, Peca J, Davison IG, Feliciano C, Deisseroth K, Augustine GJ, Ehlers MD, Feng G (2007) In vivo light-induced activation of neural circuitry in transgenic mice expressing channelrhodopsin-2. Neuron 54:205-18.

Attwell D, Laughlin SB (2001) An energy budget for signaling in the grey matter of the brain. J Cereb Blood Flow Metab 21:1133-45.

Attwell D, Buchan AM, Charpak S, Lauritzen M, Macvicar BA, Newman EA (2010) Glial and neuronal control of brain blood flow. Nature 468:232-43.

Ayling OG, Harrison TC, Boyd JD, Goroshkov A, Murphy TH (2009) Automated light-based mapping of motor cortex by photoactivation of channelrhodopsin-2 transgenic mice. Nat Methods 6:219-24.

Biber K, Laurie DJ, Berthele A, Sommer B, Tölle TR, Gebicke-Härter PJ, van Calker D, Boddeke HW (1999) Expression and signaling of group I metabotropic glutamate

receptors in astrocytes and microglia. J Neurochem 72:1671-80.

Blanco VM, Stern JE, Filosa JA (2008) Tone-dependent vascular responses to astrocyte-derived signals. Am J Physiol Heart Circ Physiol 294:H2855-63.

Boyden ES, Zhang F, Bamberg E, Nagel G, Deisseroth K (2005) Millisecond-timescale, genetically targeted optical control of neural activity. Nat Neurosci 8:1263-8.

Briers JD (2001) Laser Doppler, speckle and related techniques for blood perfusion mapping and imaging. Physiol Meas 22:R35-66.

Caesar K, Hashemi P, Douhou A, Bonvento G, Boutelle MG, Walls AB, Lauritzen M (2008) Glutamate receptor-dependent increments in lactate, glucose and oxygen metabolism evoked in rat cerebellum in vivo. J Physiol 586:1337-49.

Cauli B, Tong XK, Rancillac A, Serluca N, Lambolez B, Rossier J, Hamel E (2004) Cortical GABA interneurons in neurovascular coupling: relays for subcortical vasoactive pathways. J Neurosci 24:8940-9.

Chaigneau E, Tiret P, Lecoq J, Ducros M, Knöpfel T, Charpak S (2007) The relationship between blood flow and neuronal activity in the rodent olfactory bulb. J Neurosci 27:6452-60.

Cheng H, Duong TQ (2007) Simplified laser-speckle-imaging analysis method and its application to retinal blood flow imaging. Opt Lett 32:2188-90.

Desai M, Kahn I, Knoblich U, Bernstein J, Atallah H, Yang A, Kopell N, Buckner RL, Graybiel AM, Moore CI, Boyden ES (2010) Mapping Brain Networks in Awake Mice Using Combined Optical Neural Control and fMRI. J Neurophysiol

Devor A, Hillman EM, Tian P, Waeber C, Teng IC, Ruvinskaya L, Shalinsky MH, Zhu H, Haslinger RH, Narayanan SN, Ulbert I, Dunn AK, Lo EH, Rosen BR, Dale AM, Kleinfeld D, Boas DA (2008) Stimulus-induced changes in blood flow and 2-deoxyglucose uptake dissociate in ipsilateral somatosensory cortex. J Neurosci 28:14347-57.

DiNuzzo M, Mangia S, Maraviglia B, Giove F (2010) Glycogenolysis in astrocytes supports blood-borne glucose channeling not glycogen-derived lactate shuttling to neurons: evidence from mathematical modeling. J Cereb Blood Flow Metab 30:1895-904.

Dunn AK, Bolay H, Moskowitz MA, Boas DA (2001) Dynamic imaging of cerebral blood flow using laser speckle. J Cereb Blood Flow Metab 21:195-201.

Enager P, Piilgaard H, Offenhauser N, Kocharyan A, Fernandes P, Hamel E, Lauritzen M (2009) Pathway-specific variations in neurovascular and neurometabolic coupling in rat primary somatosensory cortex. J Cereb Blood Flow Metab 29:976-86.

Fox PT, Raichle ME, Mintun MA, Dence C (1988) Nonoxidative glucose consumption during focal physiologic neural activity. Science 241:462-4.

Fox PT, Raichle ME (1988) Focal physiological uncoupling of cerebral blood flow and oxidative metabolism during somatosensory stimulation in human subjects. Proc Natl Acad Sci U S A 83:1140-4.

Govorunova EG, Jung KH, Sineshchekov OA, Spudich JL (2004) Chlamydomonas sensory rhodopsins A and B: cellular content and role in photophobic responses. Biophys J 86:2342-9.

Grinvald A, Lieke E, Frostig RD, Gilbert CD, Wiesel TN (1986) Functional architecture of cortex revealed by optical imaging of intrinsic signals. Nature 324:361-4.

Gurden H, Uchida N, Mainen ZF (2006) Sensory-evoked intrinsic optical signals in the olfactory bulb are coupled to glutamate release and uptake. Neuron 52:335-45.

Halassa MM, Fellin T, Takano H, Dong JH, Haydon PG (2007) Synaptic islands defined by the territory of a single astrocyte. J Neurosci 27:6473-7.

Hamel E (2006) Perivascular nerves and the regulation of cerebrovascular tone. J Appl Physiol 100:1059-64.

Harrison TC, Sigler A, Murphy TH (2009) Simple and cost-effective hardware and software for functional brain mapping using intrinsic optical signal imaging. J Neurosci Methods 182:211-8.

Haydon PG, Carmignoto G (2006) Astrocyte control of synaptic transmission and neurovascular coupling. Physiol Rev 86:1009-31.

Hira R, Honkura N, Noguchi J, Maruyama Y, Augustine GJ, Kasai H, Matsuzaki M (2009) Transcranial optogenetic stimulation for functional mapping of the motor cortex. J Neurosci Methods 179:258-63.

Iadecola C, Nedergaard M (2007) Glial regulation of the cerebral microvasculature. Nat Neurosci 10:1369-76.

Ishizuka T, Kakuda M, Araki R, Yawo H (2006) Kinetic evaluation of photosensitivity in genetically engineered neurons expressing green algae light-gated channels. Neurosci Res 54:85-94.

Jakawich SK, Nasser HB, Strong MJ, McCartney AJ, Perez AS, Rakesh N, Carruthers CJ, Sutton MA (2010) Local presynaptic activity gates homeostatic changes in presynaptic function driven by dendritic BDNF synthesis. Neuron 68:1143-58.

Jolivet R, Magistretti PJ, Weber B (2009) Deciphering neuron-glia

compartmentalization in cortical energy metabolism. Front Neuroenergetics 1:4.

Kocharyan A, Fernandes P, Tong XK, Vaucher E, Hamel E (2007) Specific subtypes of cortical GABA interneurons contribute to the neurovascular coupling response to basal forebrain stimulation. J Cereb Blood Flow Metab 28:221-31.

Koehler RC, Roman RJ, Harder DR (2009) Astrocytes and the regulation of cerebral blood flow. Trends Neurosci 32:160-9.

Lecoq J, Tiret P, Najac M, Shepherd GM, Greer CA, Charpak S (2009) Odor-evoked oxygen consumption by action potential and synaptic transmission in the olfactory bulb. J Neurosci 29:1424-33.

Lee JH, Durand R, Gradinaru V, Zhang F, Goshen I, Kim DS, Fenno LE, Ramakrishnan C, Deisseroth K (2010) Global and local fMRI signals driven by neurons defined optogenetically by type and wiring. Nature 465:788-92.

Li X, Gutierrez DV, Hanson MG, Han J, Mark MD, Chiel H, Hegemann P, Landmesser LT, Herlitze S (2005) Fast noninvasive activation and inhibition of neural and network activity by vertebrate rhodopsin and green algae channelrhodopsin. Proc Natl Acad Sci U S A 102:17816-21.

Lin AL, Gao JH, Duong TQ, Fox PT (2010) Functional neuroimaging: a physiological

perspective. Front Neuroenergetics 21:2. pii: 17.

Lindauer U, Megow D, Matsuda H, Dirnagl U (1999) Nitric oxide: a modulator, but not a mediator, of neurovascular coupling in rat somatosensory cortex. Am J Physiol 277(2 Pt 2):H799-811.

Lindauer U, Leithner C, Kaasch H, Rohrer B, Foddis M, Füchtemeier M, Offenhauser N, Steinbrink J, Royl G, Kohl-Bareis M, Dirnagl U (2010) Neurovascular coupling in rat brain operates independent of hemoglobin deoxygenation. J Cereb Blood Flow Metab 30:757-68.

Liu X, Li C, Falck JR, Roman RJ, Harder DR, Koehler RC (2008) Interaction of nitric oxide, 20-HETE, and EETs during functional hyperemia in whisker barrel cortex. Am J Physiol Heart Circ Physiol 295:H619-31.

Liu X, Li C, Gebremedhin D, Hwang SH, Hammock BD, Falck JR, Roman RJ, Harder DR, Koehler RC (2011) Epoxyeicosatrienoic acid-dependent cerebral vasodilation evoked by metabotropic glutamate receptor activation in vivo. Am J Physiol Heart Circ Physiol.

Logothetis NK, Pauls J, Augath M, Trinath T, Oeltermann A (2001) Neurophysiological investigation of the basis of the fMRI signal. Nature 412:150-7.

Malonek D, Dirnagl U, Lindauer U, Yamada K, Kanno I, Grinvald A (1997) Vascular imprints of neuronal activity: relationships between the dynamics of cortical blood flow, oxygenation, and volume changes following sensory stimulation. Proc Natl Acad Sci U S A 94:14826-31.

McCaslin AF, Chen BR, Radosevich AJ, Cauli B, Hillman EM (2011) In vivo 3D morphology of astrocyte-vasculature interactions in the somatosensory cortex: implications for neurovascular coupling. J Cereb Blood Flow Metab 31:795-806.

Moriyoshi K, Masu M, Ishii T, Shigemoto R, Mizuno N, Nakanishi S (1991) Molecular cloning and characterization of the rat NMDA receptor. Nature 354:31-7.

Mukamel R, Gelbard H, Arieli A, Hasson U, Fried I, Malach R (2005) Coupling between neuronal firing, field potentials, and FMRI in human auditory cortex. Science 309:951-4.

Nawroth JC, Greer CA, Chen WR, Laughlin SB, Shepherd GM (2007) An energy budget for the olfactory glomerulus. J Neurosci 27:9790-800.

Norup Nielsen A, Lauritzen M (2001) Coupling and uncoupling of activity-dependent increases of neuronal activity and blood flow in rat somatosensory cortex. J Physiol 533:773-85.

Oberheim NA, Wang X, Goldman S, Nedergaard M (2006) Astrocytic complexity

distinguishes the human brain. Trends Neurosci 29:547-53.

Pasti L, Volterra A, Pozzan T, Carmignoto G (1997) Intracellular calcium oscillations in astrocytes: a highly plastic, bidirectional form of communication between neurons and astrocytes in situ. J Neurosci 17:7817-30.

Paulson OB, Newman EA (1987) Does the release of potassium from astrocyte endfeet regulate cerebral blood flow? Science 237:896-8.

Pellerin L, Magistretti PJ (1994) Glutamate uptake into astrocytes stimulates aerobic glycolysis: a mechanism coupling neuronal activity to glucose utilization. Proc Natl Acad Sci U S A 91:10625-9.

Pellerin L, Pellegri G, Bittar PG, Charnay Y, Bouras C, Martin JL, Stella N, Magistretti PJ (1998) Evidence supporting the existence of an activity-dependent astrocyte-neuron lactate shuttle. Dev Neurosci 20:291-9.

Nagel G, Szellas T, Huhn W, Kateriya S, Adeishvili N, Berthold P, Ollig D, Hegemann P, Bamberg E (2003) Channelrhodopsin-2, a directly light-gated cation-selective membrane channel. Proc Natl Acad Sci U S A. 100:13940-5.

Nagel G, Brauner M, Liewald JF, Adeishvili N, Bamberg E, Gottschalk A (2005) Light activation of channelrhodopsin-2 in excitable cells of Caenorhabditis elegans

triggers rapid behavioral responses. Curr Biol 15:2279-84.

Petzold GC, Albeanu DF, Sato TF, Murthy VN (2008) Coupling of neural activity to blood flow in olfactory glomeruli is mediated by astrocytic pathways. Neuron 58:897-910.

Pírez N, Wachowiak M (2008) In vivo modulation of sensory input to the olfactory bulb by tonic and activity-dependent presynaptic inhibition of receptor neurons. J Neurosci 28:6360-71.

Porter JT, McCarthy KD (1996) Hippocampal astrocytes in situ respond to glutamate released from synaptic terminals. J Neurosci 16:5073-81.

Raichle ME (1997) Food for thought. The metabolic and circulatory requirements of cognition. Ann N Y Acad Sci 835:373-85.

Rees G, Friston K, Koch C (2000) A direct quantitative relationship between the functional properties of human and macaque V5. Nat Neurosci 3:716-23.

Rossier J (2009) Wiring and plumbing in the brain. Front Hum Neurosci 3:2.

Roy CS, Sherrington CS (1890) On the Regulation of the Blood-supply of the Brain. J Physiol 85-158.17.

Scott NA, Murphy TH (2011) Glial laminar cortical architecture matches metabolic demand. J Cereb Blood Flow Metab 31:793-4.

Shi Y, Liu X, Gebremedhin D, Falck JR, Harder DR, Koehler RC (2008) Interaction of mechanisms involving epoxyeicosatrienoic acids, adenosine receptors, and metabotropic glutamate receptors in neurovascular coupling in rat whisker barrel cortex. J Cereb Blood Flow Metab 28:111-25.

Sigler A, Goroshkov A, Murphy TH (2008) Hardware and methodology for targeting single brain arterioles for photothrombotic stroke on an upright microscope. J Neurosci Methods 170:35-44.

Sineshchekov OA, Jung KH, Spudich JL (2002) Two rhodopsins mediate phototaxis to low- and high-intensity light in Chlamydomonas reinhardtii. Proc Natl Acad Sci U S A. 99:8689-94.

Sirotin YB, Das A (2009) Anticipatory haemodynamic signals in sensory cortex not predicted by local neuronal activity. Nature 457:475-9.

Sirotin YB, Hillman EM, Bordier C, Das A (2009) Spatiotemporal precision and hemodynamic mechanism of optical point spreads in alert primates. Proc Natl Acad Sci U S A 43:18390-5.

Sloan HL, Austin VC, Blamire AM, Schnupp JW, Lowe AS, Allers KA, Matthews PM, Sibson NR (2010) Regional differences in neurovascular coupling in rat brain as determined by fMRI and electrophysiology. Neuroimage 53:399-411.

Sokoloff L (1981) Relationships among local functional activity, energy metabolism, and blood flow in the central nervous system. Fed Proc 40:2311-6.

Takano T, Tian GF, Peng W, Lou N, Libionka W, Han X, Nedergaard M (2006) Astrocyte-mediated control of cerebral blood flow. Nat Neurosci. 9:260-7.

Tsai PS, Kaufhold JP, Blinder P, Friedman B, Drew PJ, Karten HJ, Lyden PD, Kleinfeld D (2009) Correlations of neuronal and microvascular densities in murine cortex revealed by direct counting and colocalization of nuclei and vessels. J Neurosci 29:14553-70.

Vaishnavi SN, Vlassenko AG, Rundle MM, Snyder AZ, Mintun MA, Raichle ME (2010) Regional aerobic glycolysis in the human brain. Proc Natl Acad Sci U S A 107:17757-62.

Vanzetta I, Grinvald A (2008) Coupling between neuronal activity and microcirculation: implications for functional brain imaging. HFSP J 2:79-98.

Vermeiren C, Najimi M, Vanhoutte N, Tilleux S, de Hemptinne I, Maloteaux JM, Hermans E (2005) Acute up-regulation of glutamate uptake mediated by mGluR5a in

reactive astrocytes. J Neurochem 94:405-16.

Wang X, Lou N, Xu Q, Tian GF, Peng WG, Han X, Kang J, Takano T, Nedergaard M. (2006) Astrocytic Ca2+ signaling evoked by sensory stimulation in vivo. Nat Neurosci 9:816-23.

Winship IR, Plaa N, Murphy TH (2007) Rapid astrocyte calcium signals correlate with neuronal activity and onset of the hemodynamic response in vivo. J Neurosci 27:6268-72.

Wyss MT, Jolivet R, Buck A, Magistretti PJ, Weber B (2011) In vivo evidence for lactate as a neuronal energy source. J Neurosci 31:7477-85.

Zhang S, Murphy TH (2007) Imaging the impact of cortical microcirculation on synaptic structure and sensory-evoked hemodynamic responses in vivo. PLoS Biol 5:e119.

Zonta M, Angulo MC, Gobbo S, Rosengarten B, Hossmann KA, Pozzan T, Carmignoto G (2003) Neuron-to-astrocyte signaling is central to the dynamic control of brain microcirculation. Nat Neurosci 6:43-50.